Journal of Wind Engineering & Industrial Aerodynamics 195 (2019) 104011

Contents lists available at ScienceDirect

Journal of Wind Engineering & Industrial Aerodynamics

journal homepage: www.elsevier.com/locate/jweia

Characteristics of thunderstorm outflows in Beijing urban area

Shi Zhang [a,c,d,*], Qingshan Yang [b,d], Giovanni Solari [c], Bo Li [a,d], Guoqing Huang [b]

[a] School of Civil Engineering, Beijing Jiaotong University, Beijing, China
[b] School of Civil Engineering, Chongqing University, Chongqing, China
[c] Department of Civil, Chemical and Environmental Engineering, University of Genoa, Genoa, Italy
[d] Beijing's Key Laboratory of Structural Wind Engineering and Urban Wind Environment, Beijing, China

ARTICLE INFO

Keywords:
Directional analysis
Downburst
Field measurement
Thunderstorm outflow
Wind properties

ABSTRACT

The study of thunderstorm outflows and their actions on structures is a dominant topic of wind engineering. This paper contributes to knowledge in this field through a systematic analysis of the thunderstorm outflows recorded by 9 anemometers installed at different heights along the 325 m high Beijing Meteorological Tower. Analyses are carried out through a directional decomposition strategy. The characteristics of a wide dataset of thunderstorm signals are analysed in a statistical environment coherent with the traditional one for synoptic winds; in this stage of the research, estimations of the mean wind speed and direction, the turbulence parameters and gust factor are carried out considering the records as disjoint from each other. Based on this choice, the results are compared with those obtained in the northern Mediterranean, providing a preliminary answer to the crucial question whether thunderstorms have similar properties in different areas, or, better, what of their properties are similar and what depend on the area itself. Besides to previous researches, the time evolution of the wind speed and direction profile is investigated with reference to a thunderstorm test case event. The systematic analysis of the full dataset of thunderstorm outflow fields is postponed to future researches.

1. Introduction

More and more attention is paid to extreme winds, mostly typhoons, tornadoes and thunderstorms, on account of the wind-induced destructive damage on structures, economy and health hazard for people (Gomes and Vickery, 1977/1978; Holmes and Oliver, 2000; Xu and Zhan et al., 2001; Su et al., 2015; Yang and Bai, 2017; Yang et al., 2018; Huang et al., 2019; Solari, 2019).

Thunderstorms are common events that can occur worldwide, even in the polar regions. At any given time approximately 2000 thunderstorms are occurring on the Earth (Choi and Hidayat, 2002a). These storms usually bring strong winds, hail and lightning, and typically cause severe property damage (Burlando et al., 2017a). Design wind velocities with mean return periods greater than 10–20 years are often associated with thunderstorm events (Letchford et al., 2002; Solari, 2014), which actually are dominant wind storms for structural design in many parts of the world. Despite this, the methods currently used to determine the wind loading of structures are still mostly based on the model introduced by Davenport (1961) over half a century ago with regard to synoptic cyclones. Thunderstorm outflows, conversely, are transient phenomena at the mesoscale (Fujita, 1985, 1990) that occur in convective conditions with nose velocity profiles (Craig Goff, 1976), totally different from those that are typical of the neutrally stratified atmospheric boundary layer (ABL). Therefore, the study of thunderstorm outflows and their loading of structures is a matter of vital importance for modern wind engineering and construction safety (Solari, 2014).

Recently, several studies have been performed in wind engineering with reference to extracting the wind parameters of major interest for evaluating the wind loading and response of structures to thunderstorm outflows (Letchford et al., 2002), based on the data detected in different areas of the world. Choi (2000, 2004); Choi and Hidayat 2002a, 2002b described the results of a monitoring program in Singapore, which paid particular attention on the definition and values of the gust factor. A deterministic–stochastic hybrid model of thunderstorm downbursts was presented by Chen and Letchford (2004), in which the downburst wind speed was expressed as the summation of a deterministic mean part and a stochastic fluctuation. Durañona et al. (2007) analysed the time evolution of the vertical profile of the mean wind velocity and of the turbulence properties of transient events registered in the north-European coastal areas. Orwig and Schroeder (2007) investigated the space-time properties of the rear-flank downdraft of a super-cell and of a derecho detected in a thunderstorm outflow experiment conducted in 2002 in

* Corresponding author. School of Civil Engineering, Beijing Jiaotong University, Beijing. China.
E-mail address: 10231097@bjtu.edu.cn (S. Zhang).

https://doi.org/10.1016/j.jweia.2019.104011
Received 9 May 2019; Received in revised form 5 October 2019; Accepted 7 October 2019
Available online 23 October 2019

Lubbock, Texas. Inspecting the same rear-flank downdraft, Holmes et al. (2008) decomposed its velocity into a slowly-varying mean part and a residual turbulent fluctuation whose characteristics were examined without considering directionality. Similar evaluations were reported by Jarvi et al. (2007) with reference to a downburst that occurred in 2004 at the SMEAR II Station in Finland. Lombardo et al. (2014) investigated some thunderstorms detected in Lubbock in order to elucidate their properties relevant to wind engineering. Gunter and Schroeder (2015) depicted high-resolution field measurements of thunderstorm outflows carried out at the Texas Tech University by means of surface instruments and mobile Doppler radars. Solari et al. (2015) and Zhang et al. (2018a) analysed the statistical properties of thunderstorm outflows according to a high-resolution database gathered by a wind monitoring network in the northern Mediterranean ports. In addition, in order to overcome the shortcomings of classical signal decompositions (Chen and Letchford, 2004), which ignores directional shifts, a novel directional decomposition strategy of the wind speed was formulated by Zhang et al. (2019). It opens the doors to a robust comparison between thunderstorm outflows and synoptic winds in terms of wind speed, wind loading and dynamic structural response.

China, a country in East Asia having the world's largest population and covering approximately 9,600,000 square kilometres, also frequently experiences intense thunderstorms. For instance, at about 2132 BT, June 1, 2015, the 'Oriental Star' cruise from Nanjing to Chongqing suffered a severe stormy weather, which was confirmed to be a sudden squall line of downbursts, when it was sailing in the Yangtze River near Jianli County, resulting in 442 people killed (Duan et al., 2017). Thunderstorms represent also the main disastrous weather bringing strong winds in the national capital Beijing (Fu and Guo, 2007). On July 22, 1997, 27 houses were destroyed and dozens of trees up to 40 cm in diameter were blown up by a thunderstorm downburst (Liu, 2001). This sudden thunderstorm that struck Beijing with hailstones and the peak wind speed of more than 20 m/s at around 2000 BT, August 23, 2001 interrupted the Chinese and English football match of the World University Games; besides, it also brought serious damage to facilities and disruptions in electric power (Qin et al., 2006; Fu and Guo, 2007).

Meteorologists have made some achievements in the study of this phenomenon in Beijing. Based on the observational data of meteorological instruments, the thunderstorms in Beijing have strong local features, which mainly arise from the intense development of local convective systems, while large scale thunderstorm winds caused by large scale weather systems are rare. Besides, the occurrence of thunderstorms in Beijing area is restricted by topography, namely they are more likely to occur in wide, flat areas than near mountainous areas (Qin et al., 2006). Based on local statistics, for 134 thunderstorm gales from 1998 to 2007 in Beijing area, it is known that most of them were accompanied by downbursts and some of them broke out while hails were falling (Liao et al., 2009).

Despite these and many other analyses, to the authors' knowledge, research about the properties of thunderstorms relevant to the wind loading of structures in Beijing and partly in China (Huang et al., 2019) is still lacking. The Beijing 325 m high meteorological tower (Li et al., 2009; Tian et al., 2011; Hui et al., 2017) - along which 11 ultrasonic anemometers are mounted at nine different heights from 8 m to 280 m, capable of detecting high-resolution data with 10 Hz sampling frequency from 2013 - provides a unique opportunity to shed new light on this crucial issue, to detect thunderstorm records, and to study their characteristics from the perspective of wind engineering. The presence of anemometers installed at different levels on the same tower makes it possible to study the time evolution of the wind speed profile related to thunderstorm outflows, a topic investigated in some detail in the Mediterranean (Solari et al., 2015; Zhang et al., 2018a, 2019) due to the dominant presence of single anemometers.

In addition, performing comparative analyses of the wind properties during thunderstorm outflows, in particular the ones detected in China and in the northern Mediterranean, provides a preliminary answer to a question judged by most as fundamental to build a model of this phenomenon shared worldwide: have thunderstorms in different areas similar properties? Or, better, what thunderstorm properties may be considered as universal ones and what instead depend on the area and/or on the meteorological condition in which they occur? Holmes (2019) recently showed that in Australia the properties of thunderstorms relevant to the wind loading of structures depend on latitude, enhancing the crucial role of the above issue.

In this framework, section 2 illustrates the main properties of the measurement site and observations. The characteristics of the Beijing climate and the wind speed statistical properties based on the ultra-sonic anemometers on the tower are introduced briefly in section 3. Section 4 describes the criterion by means of which different intense wind events are separated and thunderstorm outflows are extracted and catalogued; it also provides additional elements on the direction, seasonality and hour of the daily occurrence of these events. Section 5 recalls the directional method applied to decompose the thunderstorm outflow signals into component terms. Accordingly, section 6 analyzes the slowly-varying mean wind speed and direction, the turbulence parameters and the gust factor; in this stage of the research, likewise in the Mediterranean area, the examined records are dealt with as disjoint from each other also to facilitate the comparison between the two datasets. Section 7 describes the time evolution of the wind speed and direction profile with reference to a thunderstorm test case event. Section 8 summarizes the main conclusions and draws some prospects for the prosecution of this research, first of all with reference to a systematic analysis and interpretation of the most relevant thunderstorm outflows as simultaneously detected by the anemometers installed at different levels along the tower.

2. Measurement site and observations

Beijing is one of the largest cities in the world; since 1978, its urban area and population exhibited an exponential growth according to which, by 2016 it reached 21.73 million residents. The 325 m high meteorological tower (39°58′N, 116°2′E) is a guyed mast with regular triangle cross-section; it is situated between the Northern 3rd Ring Road and the Northern 4th Ring Road of Beijing city; it was set up in 1978 by the Institute of Atmospheric Physics (IAP) of the Chinese Academy of Sciences (CAS). The height of its base is about 48.63 m above the sea level. Fig. 1 shows the picture of the meteorological tower where a number of anemometers was installed **(a)** and the satellite picture of the landforms around it (the red circle) **(b)**. As shown in Fig. 1 **(b)**, there is almost no high rise structure within 1 km range of the tower, except for some residential buildings, about 60 m high, which are located 100 m away from the tower in the south direction. The site around the tower can be regarded as terrain C (urban area) according to the Chinese National Load Code (GB50009-2012).

Fig. 2 shows the location of thirty vane anemometers (EC9-1 with high resolution, 0.1 m/s, produced by the Changchun Meteorological Instrument Research Institute, China) which were installed on the tower at fifteen different levels in order to measure the mean wind speed data with a sampling rate of 0.05 Hz; in addition, there are eleven three-channel ultrasonic anemometers mounted at nine different heights along the tower, namely 8, 16, 32, 47, 64, 80, 140, 200, and 280 m (Xu and Zhang, 2019). Finally, at 32 and 64 m height there are two ultrasonic anemometers mounted at the same heights with different orientations (north and west), for validating the measured fluctuating speeds. To check the reliability of instruments, the measured wind speeds at each height are firstly averaged within 10-min periods and compared with the results provided by the cup-type anemometers; thus, the fidelity of instruments is well examined. To avoid the interference effects of the tower itself on the wind, the anemometers are fixed 1.5 m away from the tower on the north side, which is exposed to the dominant synoptic winds in Beijing during winter and spring. Hence, this meteorological tower is the best observation station to study the urban boundary layer and the urban most intense storms in Beijing city.

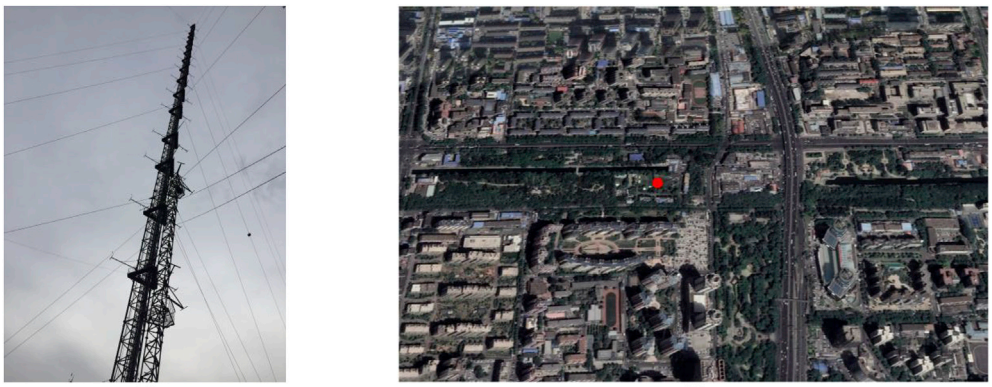

(a) (b)

Fig. 1. Picture of the Beijing 325 m meteorological tower (a) and satellite image of landforms around it (b).

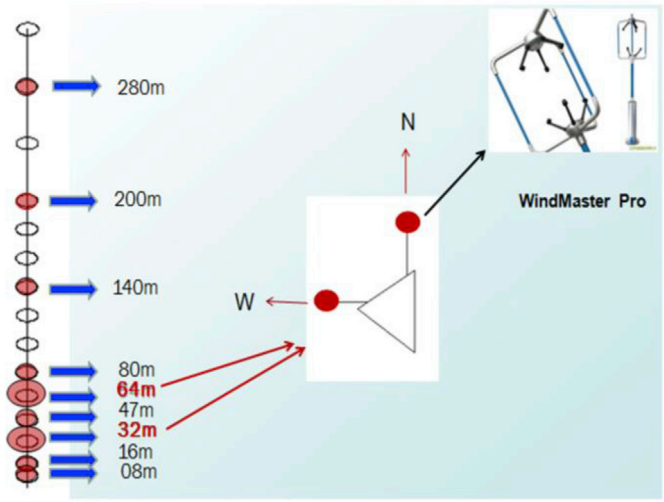

Fig. 2. Arrangement of ultrasonic anemometers on the Beijing 325 m high meteorological tower.

The data provided by the three-axial ultrasonic anemometers is stored into a database in terms of three instantaneous wind speed components (V_X, V_Y, V_Z), according to the geophysical coordinate system, where V_X is directed from South to North, V_Y from East to West, and V_Z is vertical and positive upwards. All these ultrasonic anemometers continuously collect wind speed data simultaneously with a sampling rate of 10 Hz.

3. Beijing wind climate

There are two main characteristics of China's climate: the climate is complex and diverse, and the monsoon climate is remarkable. Due to the vastness of China, its climate is manly divided into 5 areas as shown in Fig. 3. The typical monsoon climate region in the eastern part of China is characterized by a temperate monsoon climate, a subtropical monsoon climate, and a tropical monsoon climate from north to south. The temperate continental climate is distributed in the Northwest China. The Tibetan Plateau is characterized by a plateau mountain climate.

Beijing, the capital of China, lies northwest of the north China plain with a total area of 16,410.54 square kilometres, as shown in the pentagram in Fig. 3. The wind system of this city is dominated by the monsoon-influenced humid continental climate, characterized by hot, humid summers due to the East Asian monsoon, and by cold, windy, dry winters that reflect the influence of the vast Siberian anticyclone. Spring and autumn are seasons of transition and minimal precipitation. The monthly daily average temperature in January is −5~-4 °C, while in July it is 26.2 °C for the plain region. The spatial distribution of annual precipitation is uneven, and the precipitation is close to 3/4 of the annual precipitation from June to August.

This area is not affected by typhoons or tornados. On the other hand, there are frequent occurrences of thunderstorms. The winds produced by thunderstorm events are relatively stronger and more turbulent than those produced by monsoon winds and extra-tropical cyclones. Therefore, thunderstorm winds are important sources of strong winds in Beijing, and their main characteristics related to the wind loading of structures are dominant for the structure design.

The data detected by the 140 m anemometer on the Beijing 325 m high meteorological tower in 2013–2017 is used to preliminarily evaluate the local statistical properties of the wind speed. The monthly maximum mean wind speeds in 10-min time intervals $\overline{U}_{max}$ from this anemometer are shown in Fig. 4. Their range is between 10 and 25 m/s. The maximum 10-min mean wind speeds occur generally in May for 2014, 2016 and 2017. However, in 2013 and 2015, they occurred in July and February, respectively. The overall values are relatively higher in spring and winter, which is consistent with the long-term meteorological statistical results.

Horizontal wind roses for different seasons according to the data detected by the anemometer at 140 m height in 2013 are shown in Fig. 5. It shows that the dominant wind direction is northwest and southeast, which is consistent with the characteristics of Beijing's climate; almost all the strong winds larger than 8 m/s come from the northwest direction; strong winds frequently occur in spring and winter, while in summer the wind is weak; the northwest wind is dominant in spring, autumn and winter, while the southeast wind occurs more frequently in summer than in the other seasons.

4. Separation and classification of thunderstorm outflows

Based on the characteristics of the Beijing wind climate described in the previous section, typhoons never occur in this area and thunderstorms are among the most frequent disastrous weather phenomena, especially in summer (Liao et al., 2009). A thorough examination of the large amount of the collected data reveals that intense wind events can be separated into three families characterized by different statistical properties similar to the ones that occur in the mid-latitude region in the northern Mediterranean (De Gaetano et al., 2014; Zhang et al., 2018a and 2018b):

(1) stationary Gaussian events with relatively large mean wind velocities and small gust factors; they usually correspond to synoptic neutral atmospheric conditions and are here referred to as synoptic storms, namely monsoons and extra-tropical cyclones or large depression systems;

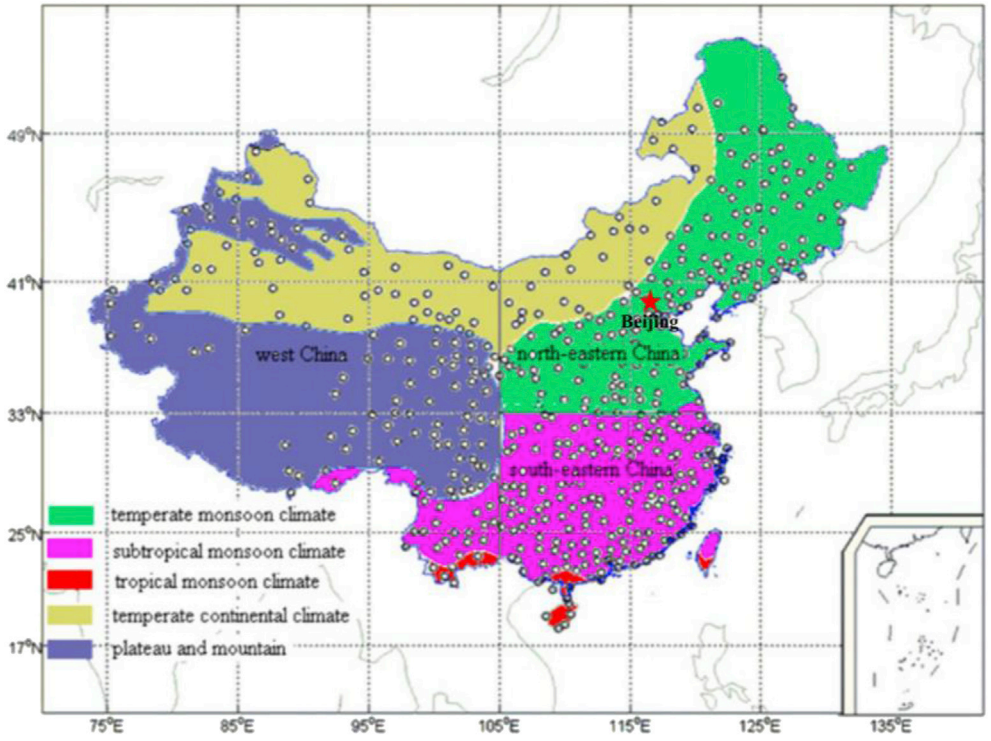

Fig. 3. Distribution of climate regions in China (Song et al., 2011).

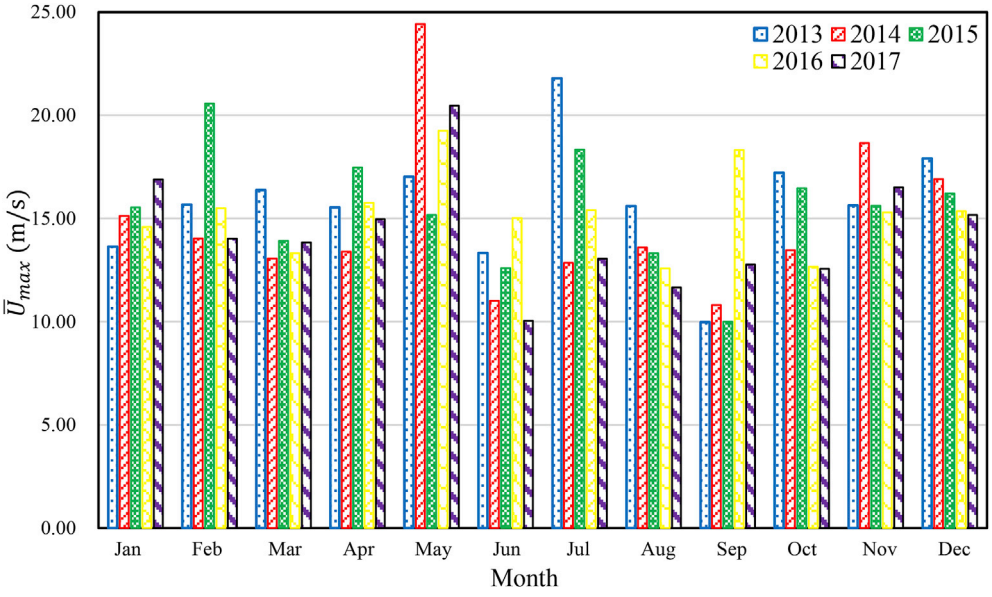

Fig. 4. Monthly maximum mean wind speed.

(2) non-stationary non-Gaussian events with relatively small mean wind velocities, large and quite isolated peaks, and high gust factors; they are here referred to as thunderstorms outflows;
(3) nearly-stationary non-Gaussian events with relatively small mean wind velocities, large and repeated peaks, and moderately high gust factors; probably they occur in unstable atmospheric conditions and are here referred to as intermediate events or gust fronts (Kasperski, 2002).

To achieve the separation and classification of different intense wind events as easily and efficiently as possible, a semi-automated procedure proposed by De Gaetano et al. (2014) and improved by Zhang et al. (2018a) is applied to the records with the horizontal 1-s peak wind velocity $\widehat{U}$ greater than 15 m/s. The choice of this threshold is coherent with thunderstorm analyses carried out by these and other authors (Choi, 2000, 2004; Durañona et al., 2007) and with the tradition of evaluating the parameters of synoptic events by collecting all records that satisfy the requirement of neutral atmospheric conditions (Solari and Piccardo, 2001; Solari and Tubino, 2002), these including several phenomena of limited engineering interest. The alternative approach of restricting analyses to thunderstorm outflows with higher peak values (Geerts, 2001; Lombardo et al., 2014) improves the information related to the phenomena of major engineering interest, but reduces the statistical representativeness of the results.

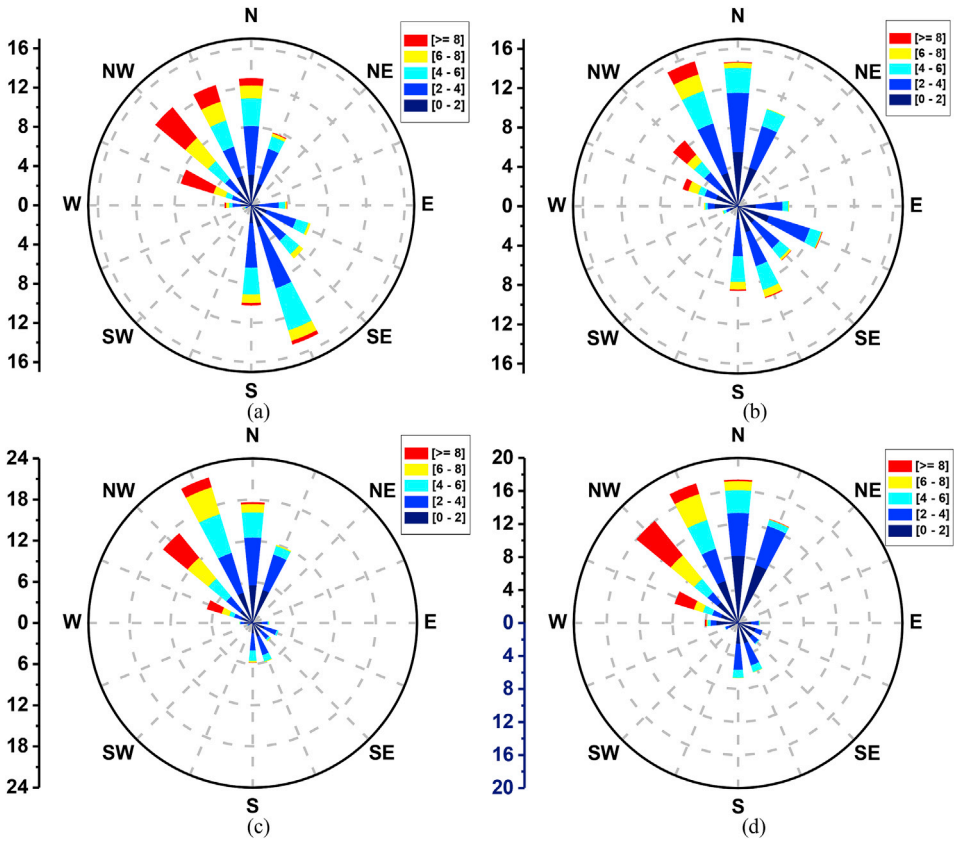

Fig. 5. Horizontal wind roses in different seasons at 140 m in 2013: (a) Spring; (b) Summer; (c) Autumn; (d) Winter.

The semi-automated procedure used herein involves a mix of quantitative controls and qualitative judgments. The quantitative controls are based on the comparison between the detected values of the gust factors referred to different time periods (Burlando et al., 2018) and reference values evaluated assuming that intense wind speeds occur in neutral atmospheric conditions during synoptic storms (ESDU, 1993; GB50009-2012).

As mentioned in the previous section, there are 11 ultra-sonic anemometers installed at nine different heights along the tower. The above procedure was applied to the data recorded by the 9 ultra-sonic anemometers on the north side of the tower during the period 2013–2017. After the quantitative controls, over 97.5% of the records related to intense wind events were automatically identified as synoptic events. The remaining ones were submitted to qualitative judgments mainly based on 10-min, 1-h and 10-h records centred around the peak wind speed. The information about temperature made a great contribution to this judgement, since it generally presents a clear decrease during the passage of the gust front of a thunderstorm outflow (Huang et al., 2019). In addition, the availability of weather records in Beijing was used as a reference information. Accordingly, thunderstorm outflows and intermediate events were separated with reasonable confidence.

Three typical 1-h time history records registered by the 280 m anemometer high, which correspond to a synoptic storm ($\widehat{U}$=23.01 m/s), a thunderstorm outflow ($\widehat{U}$=29.80 m/s) and an intermediate event ($\widehat{U}$=16.20 m/s), are shown in Figs. 6, 7 and 8, respectively. The pictures **(a), (b)** and **(c)** show the time-series of the wind speed, wind direction

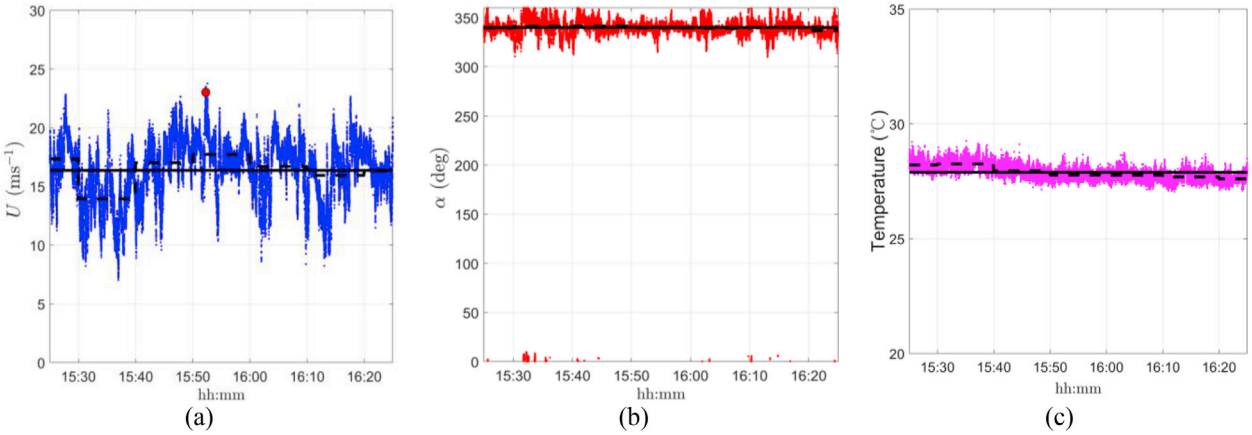

Fig. 6. Synoptic wind recorded on 11 May 2017 by the 280 m anemometer high: (a) 1-h wind speed time-series; (b) 1-h wind direction time-series; (c) 1-h temperature time-series.

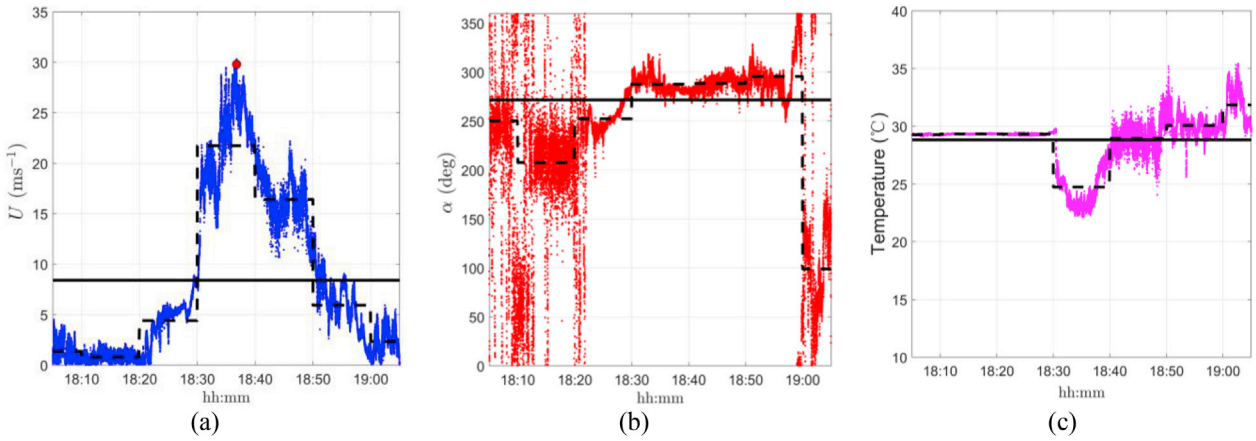

Fig. 7. Thunderstorm outflow recorded on 07 September 2016 by the 280 m anemometer high: (a) 1-h wind speed time-series; (b) wind direction time-series; (c) 1-h temperature time-series.

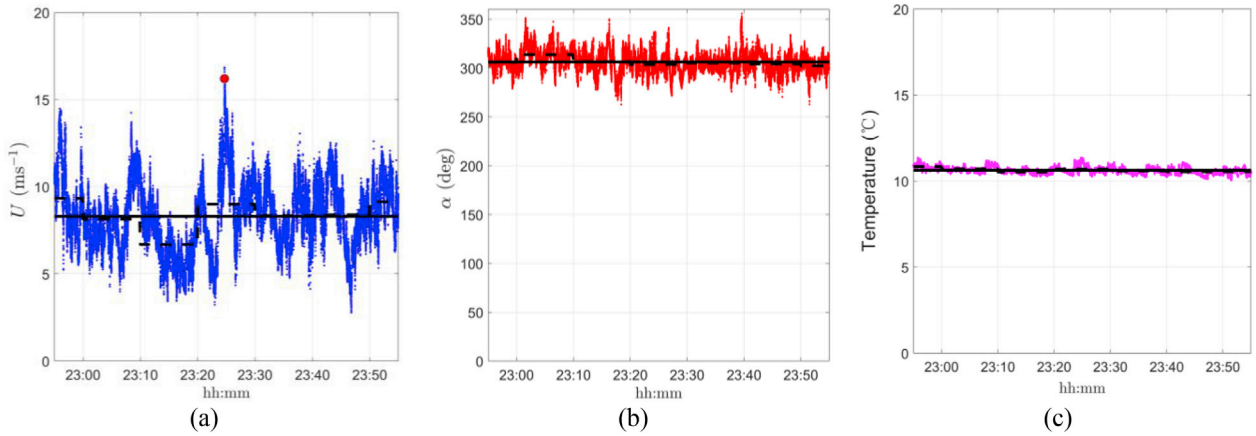

Fig. 8. Intermediate event recorded on 02 December 2015 by the 280 m anemometer high: (a) 1-h wind speed time-series; (b) wind direction time-series; (c) 1-h temperature time-series.

and temperature raw data, respectively, and their mean values over 1-h (solid lines) and 10-min (dotted lines) periods. In pictures **(a)**, the 1-s peak wind speed (red circles) is also shown, which is obviously smaller than the instantaneous peak.

On the whole, dealing with single records, this approach led to extract NTR = 314 disjoint non-stationary records that were traced back to convective conditions and thunderstorm outflows. Of course, since the same thunderstorm may be detected by several anemometers simultaneously, the number of thunderstorm events NTE = 70 is smaller than NTR = 314.

This analysis points out a main difference with respect to the analogous study carried out in the Northern Mediterranean area: in the latter the anemometers are distributed in different positions whereas in Beijing they are located along the same tower. This gives rise to a delicate issue: during a thunderstorm, not all the wind speed records, analysed above separately, usually have a peak wind speed above 15 m/s and non-stationary properties. Accordingly, the overall number NTO of the records detected during thunderstorms, NTO = 630, is greater than NTR = 314.

This aspect leads to a complication: the study of the most relevant thunderstorm records dealt with as disjoint includes NTR = 314 signals; the study of the most relevant thunderstorm events involves all the NTO = 630 records detected at different heights independently of their singular properties.

Table 1 summarizes the selected records and points out the above remarks. The columns "10-min", "1-h" and "10-h" provide, for each anemometer height, the number of events that can be recognized as non-stationary on 10-min, 1-h and 10-h periods respectively (Burlando et al., 2018).

Table 1
Number of thunderstorm events and records examined.

Anemometer No.	*h* (m)	10-min	1-h	10-h	NTR	NTE	NTO
1	8	5	5	0	10	70	70
2	16	7	8	1	16		70
3	32	12	12	1	25		70
4	47	11	19	2	32		70
5	64	16	24	1	41		70
6	80	12	25	3	40		70
7	140	10	38	3	51		70
8	200	8	38	1	47		70
9	280	5	45	2	52		70
Total		86	214	14	314	70	630

The comparison between the data provided in Table 1 for the Beijing urban area and the analogous data provided in Table 2 by Burlando et al. (2018) for the Mediterranean area indicates, in the former area, a major number of long events. In reality, limiting the comparison to the first 10–30 m above the ground level (AGL), where most of the latter data are measured, the typical duration of the gust front passage in Beijing is slightly longer than in the Mediterranean. Longer durations occur above 30 m AGL, where a few data are available in the Mediterranean.

The information provided in Table 1 is completed in Table 2 by

Table 2
Classes of membership of the peak wind velocity of thunderstorm outflows.

$\hat{U}$ (m/s)	Anemometer (m)									
	8	16	32	47	64	80	140	200	280	ALL
15–20	7	12	16	22	30	25	27	26	31	196
20–25	3	3	7	8	7	12	14	11	12	77
25–30	–	1	2	2	3	2	7	7	6	30
30–35	–	–	–	–	1	1	2	2	2	8
35–40	–	–	–	–	–	–	1	1	1	3
ALL	10	16	25	32	41	40	51	47	52	**314**

separating the transient records into five groups as a function of the 1-s peak wind speed (m/s), namely $15 \leq \hat{U} < 20$, $20 \leq \hat{U} < 25$, $25 \leq \hat{U} < 30$, $30 \leq \hat{U} < 35$ and $35 \leq \hat{U} < 40$. This new table points out that thunderstorm records whose 1-s peak wind speed exceeds 20 m/s are detected by all the anemometers from 8 m to 280 m, while only the anemometers higher than 64 m detect thunderstorm records whose 1-s peak wind speed exceeds 30 m/s. Studies are in progress in order to interpret these data with regard to the time-space evolution of the wind speed profile concurrent with their detection.

Fig. 9 shows the distribution of the 70 thunderstorm events reported in Table 1 with reference to their daily occurrence. Accordingly, similar to the observations in the northern Mediterranean (Burlando et al., 2018), thunderstorm frequently occur in the warmer hours of the day, namely in the afternoon and in the first half of the night.

5. Directional decomposition of the wind speed

With respect to the classical approach used in literature (Holmes et al., 2008; Solari et al., 2015; Zhang et al., 2018a), a new decomposition strategy (Zhang et al., 2019) is herein applied in order to properly account for wind direction shifts. The two horizontal components (V_X, V_Y) of the wind speed are decomposed into a couple of slowly-varying mean wind speeds $(\overline{V}_X, \overline{V}_Y)$ and residual fluctuations (V_X', V_Y') by a moving average filter with period $T = 30$ s (Riera and Ponte, 2012; Solari et al., 2015), in which, V_X' and V_Y' are the fluctuations in the zonal (S-N) and meridional (E-W) directions related to $\overline{V}_X$ and $\overline{V}_Y$ as shown in Fig. 10 **(a)**.

The slowly-varying horizontal mean wind velocity vector is defined in terms of the wind speed and direction:

$$\overline{u}(t) = \sqrt{\overline{V}_X^2(t) + \overline{V}_Y^2(t)}, \quad \overline{\alpha} = 270 - \text{atan2}(\overline{V}_Y / \overline{V}_X) \tag{1}$$

where $\overline{\alpha} \in [0 : 360]$ is expressed according to the geographical notation and atan2 is the generalized arc-tangent function. The residual fluctuations V_X' and V_Y' are then projected onto a new Cartesian reference system (x, y), where the x-axis is aligned with $\overline{u}(t)$. Thus:

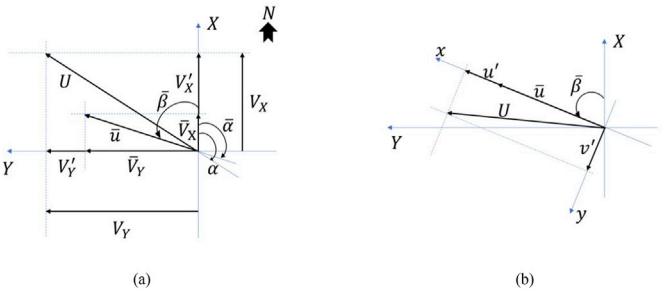

Fig. 10. Directional decomposition of the anemometric data.

$$\begin{aligned} u'(t) &= -V_X'(t)\sin\overline{\alpha}(t) - V_Y'(t)\cos\overline{\alpha}(t) \\ v'(t) &= V_X'(t)\cos\overline{\alpha}(t) - V_Y'(t)\sin\overline{\alpha}(t) \end{aligned} \tag{2}$$

u' and v' being referred to as the longitudinal and lateral turbulent fluctuations as shown in Fig. 10 **(b)**. In turn, these quantities are rewritten as the product of their slowly-varying standard deviations (σ_u, σ_v), evaluated over the same period T of the moving average, multiplied by a couple of reduced longitudinal and lateral turbulent fluctuations $(\tilde{u}', \tilde{v}')$. Accordingly, the longitudinal and lateral components of the wind velocity are expressed as:

$$\begin{aligned} u(t) = \overline{u}(t) + u'(t) = \overline{u}(t)[1 + I_u(t)\tilde{u}'(t)] = \overline{u}_{max}\gamma_u(t)[1 + \overline{I}_u\mu_u(t)\tilde{u}'(t)] \\ v(t) = v'(t) = \overline{u}(t)I_v(t)\tilde{v}'(t) = \overline{u}_{max}\gamma_u(t)\overline{I}_v\mu_v(t)\tilde{v}'(t) \end{aligned} \tag{3}$$

where $\overline{u}_{max}$ is the maximum value of $\overline{u}$ whereas γ_u is a non-dimensional function of t that describes the slow variation of $\overline{u}$, being $\gamma_{u,max} = 1$; $I_u(t) = \sigma_u(t)/\overline{u}(t) = \overline{I}_u\mu_u(t)$ and $I_v(t) = \sigma_v(t)/\overline{u}(t) = \overline{I}_v\mu_v(t)$ are the longitudinal and lateral turbulence intensities; $\overline{I}_u$ and $\overline{I}_v$ are the average values of I_u and I_v in $\Delta T = 10$ min, whereas μ_u and μ_v are non-dimensional functions of t that describe the slow variation of I_u and I_v, being $\overline{\mu}_u = \overline{\mu}_v = 1$.

Finally, the gust factor is expressed by the relationship $G_u = \hat{u}/\overline{u}_{max}$, where $\hat{u}$ is the peak longitudinal velocity (averaged over the period $\tau = 1$ s). Zhang et al. (2019) provided a detailed comparison between the classical decomposition rule and the new one described above.

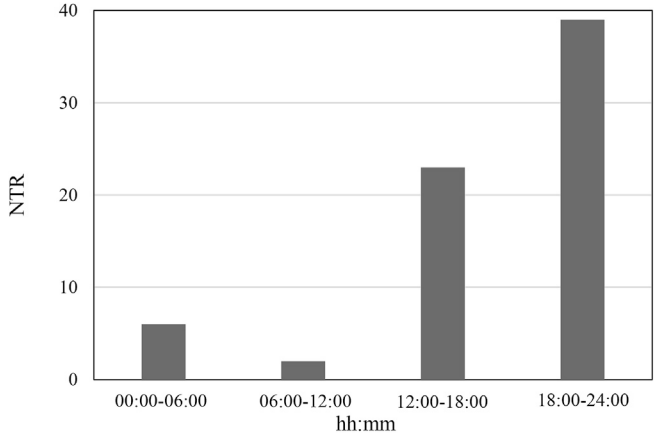

Fig. 9. Number of thunderstorm outflow records detected at different hours of the day.

6. Statistical properties of thunderstorm outflows

Based on the Beijing meteorological tower described in section 4, there are 314 thunderstorm outflow recordings available now. Each one of them has been first decomposed into component signals by means of the directional rule described in section 5. Subsequently, the components signals have been analysed statistically, both considering the single anemometers at different heights and the whole of the registrations. The final aim of this study is to inspect the most relevant properties of the thunderstorm outflows detected in the Beijing urban area and to compare this information with the properties of the thunderstorm outflows detected in the northern Mediterranean.

This comparison is quite delicate due to the different properties of the two datasets. In addition to the different geographical positions, the neighboring terrains are totally diverse. In Beijing the tower is placed in a flat urban area whereas in the Mediterranean the anemometers are distributed along the coast, with the sea on one side, over which most of the thunderstorms are originated, and an urban exposure inland, often involving complex topographic features. Besides, in Beijing the anemometers are uniformly distributed between 8 and 280 m height whereas in the Mediterranean most of them are placed between 10 and 30 m height, with only a few ones between 30 and 80 m height. Under this point of view the most probative comparison with the Mediterranean dataset should be limited to the 3–4 Beijing anemometers closest to the ground.

In this framework, the organization of this section deals with the slowly-varying mean wind speed (section 6.1) and direction (section 6.2), the turbulence intensity (section 6.3), the reduced turbulent fluctuations (section 6.4), their integral length scales and power spectral densities (section 6.5), the turbulence intensity modulation (section 6.6), and the gust factor (section 6.7).

It is worth noticing that the above sections provide and discuss data dealt with as disjoint, putting together records detected during the same thunderstorm event with data detected in different events. Accordingly, such data should be interpreted in a probabilistic framework, height by height, without any attempt to speculate on the reconstruction of the vertical profile. This issue is discussed in section 7 with reference to a thunderstorm test case whereas a detailed investigation and discussion about the time evolution of the wind speed and direction profile is postponed to future papers currently in progress.

6.1. Slowly-varying mean wind velocity

The records labelled here as thunderstorm outflows are characterized by a prominent peak whose duration has a dominant role in the wind loading and response of structures (Kwon and Kareem, 2009). Such peak is best described by the slowly varying mean wind velocity $\overline{u}(t)$ or, even better, by the non-dimensional function $\gamma_u(t)$ (Eq. (3)).

Fig. 11 **(a)** shows the mean value of the non-dimensional function $\gamma_u(t)$ for the thunderstorm records detected by each anemometer. The solid lines correspond to the first 4 anemometers, at heights comparable with those of the anemometers in the Mediterranean area, whereas the dashed lines correspond to higher instruments. All the diagrams identify the essential features of a ramp-up and -down in the wind speed corresponding to the passage of a gust front.

It is apparent that on increasing the height above the ground, the duration of the most intense part of the thunderstorm outflows increases. This confirms the remarks already pointed out with reference to Table 1, according to which the number (NTR) of the events belonging to the 10-min and 1-h family are similar for the 3 anemometers closest to ground and both of them are not so numerous. For the anemometers between 47 and 80 m height, the number (NTR) of the events belonging to the 1-h family is almost twice those of the 10-min family, whereas for the 3 highest anemometers the duration of the intense part further increases.

Fig. 11 **(b)** shows the typical diagram of a $\gamma_u(t)$ function and depicts the criterion introduced by Solari et al. (2015) to evaluate the passage duration of the gust front. $T_i = -t_i$ and $T_d = t_d$ are referred to as the thunderstorm increasing (ramp-up) and decreasing time period, respectively, t_i and t_d being the conventional values of t for which the most intense part of the thunderstorm begins and finishes; $T_t = T_i + T_d$ is the total duration of the most intense part of the thunderstorm; $\gamma = 0.6$ is a threshold corresponding to a wind velocity pressure equal to 36% of its maximum value. Table 3 shows the mean value, the coefficient of variation (cov) and the minimum value of T_i, T_d and T_t for all the thunderstorm records detected by each anemometer and by the whole monitoring system, confirming the trend according to which the passage duration of the gust front increases on increasing the height. In addition, it shows that the overall mean values of T_i, T_d and T_t are 143, 190 and 333s respectively. The minimum values of T_i, T_d and T_t, about 9, 11 and 32s respectively, indicate the possibility that some thunderstorm outflows occur with very rapid variations of the wind velocity.

The comparison between the values reported in Table 3 and the corresponding values reported in Table 7 of the paper by Solari et al. (2015) shows that close to the ground the passage duration of the gust fronts on the Beijing tower is considerable lower than that observed in the northern Mediterranean at similar heights. The passage duration of the gust front in the Mediterranean (close to the ground) is similar to that observed at the Beijing tower at intermediate heights.

All this matter deserves further examinations taking into account the time evolution of the mean wind speed profile. Some preliminary analyses are carried out in Section 7 for a single thunderstorm outflow whereas more systematic studies will be carried out in papers currently in progress.

6.2. Slowly-varying mean wind direction

The slowly-varying mean wind direction $\overline{\alpha}$ (Eq. (1)) of the thunderstorm outflow records considered here exhibits complex and varied trends. By way of example, Fig. 12 **(a)** shows a slowly-varying mean wind speed record, $\overline{u}(t)$, in which a rapid variation takes place for a relatively short time period. On the other hand, Fig. 12 **(b)** shows that the corresponding slowly-varying mean wind direction, $\Delta\overline{\alpha}$, exhibits a sudden shift that anticipates the peak and lasts for a longer time period.

Referring to the ensemble of the transient records herein analysed, Table 4 provides an attempt to quantify the maximum rate of change of the slowly-varying mean wind direction, $\Delta\overline{\alpha}$, in the 30-min period centred around the maximum wind speed. Most of the examined events (67%) has a rate of change $\Delta\overline{\alpha}$ larger than 90 deg. The choice of the most effective period in which the directional shift has to be evaluated calls for further studies (Zhang et al., 2019).

Fig. 13 shows the peak wind speed $\widehat{U}$ as a function of the direction shift $\Delta\overline{\alpha}$. Three remarks stand out: 1) none of the examined events is characterised by $\Delta\overline{\alpha} < 15$ deg, which corresponds to nearly straight winds; 2) only one record exceeds the peak wind speed $\widehat{U} = 30$ m/s in the range of $\Delta\overline{\alpha} > 145$ deg; 3) no apparent correlation emerges between $\widehat{U}$ and $\Delta\overline{\alpha}$. Despite this last remark, 10 of the 11 most intense events,

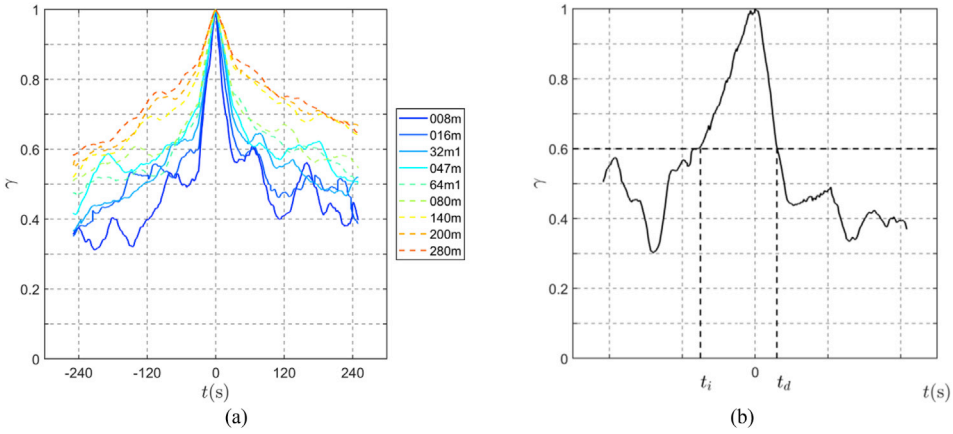

Fig. 11. Normalized slowly-varying mean wind velocity: (a) men values for each anemometer; (b) typical diagram of the γ function for a wind speed record.

Table 3
Mean values, covs and minimum values of T_i, T_d and T_t for all the thunderstorm outflow records.

Anem. No.	Mean(T_i) (s)	cov(T_i) (s)	Min(T_i) (s)	Mean(T_d) (s)	cov(T_d) (s)	Min(T_d) (s)	Mean(T_t) (s)	cov(T_t) (s)	Min(T_t) (s)
1	35.01	0.57	19.10	40.64	0.67	12.80	75.65	0.41	32.10
2	54.47	0.82	18.20	59.66	0.73	14.50	114.13	0.63	33.30
3	59.61	0.96	21.30	74.08	1.09	17.70	133.69	0.90	39.80
4	76.41	0.83	9.20	87.96	0.84	14.90	164.37	0.71	32.60
5	74.96	0.84	16.30	102.12	0.72	21.00	177.08	0.65	40.00
6	94.34	0.93	19.00	105.48	0.81	10.90	199.82	0.68	38.50
7	179.29	0.94	23.40	226.36	0.82	20.20	405.66	0.75	62.80
8	226.41	1.20	19.10	302.64	1.21	20.20	529.05	1.12	42.20
9	248.18	0.94	24.00	364.35	0.87	19.00	612.53	0.71	44.40
All	143.24	1.26	9.20	189.54	1.27	10.90	332.79	1.13	32.10

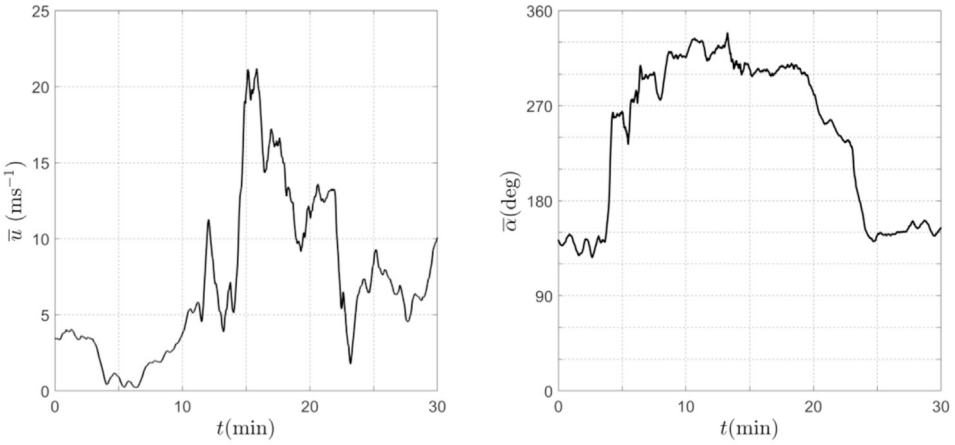

(a) (b)

Fig. 12. 30-min slowly-varying mean wind velocity (a) and direction (b) centred around the peak wind velocity during a thunderstorm outflow occurred on June 10, 2016 as detected by the anemometer at 80 m height.

Table 4
Classes of membership of the maximum shift of the slowly-varying mean wind direction in the 30-min period centred around the peak wind speed.

	Maximum direction shift (deg)				
h (m)	$\Delta\overline{\alpha}\leq 45$	$45 < \Delta\overline{\alpha}\leq 90$	$90 < \Delta\overline{\alpha}\leq 180$	$\Delta\overline{\alpha} > 180$	All
8	0	0	3	7	10
16	0	4	3	9	16
32	1	4	7	13	25
47	0	8	15	9	32
64	2	4	21	14	41
80	2	8	18	12	40
140	5	18	22	6	51
200	2	19	18	8	47
280	5	20	13	14	52
All	17 (6%)	85 (27%)	120 (38%)	92 (29%)	314

those exceeding $\widehat{U} = 30$ m/s, involve directional shifts in the range between 35 and 145 deg.

6.3. Turbulence intensity

The longitudinal and lateral slowly-varying turbulence intensities, I_u and I_v, are defined through Eq. (3). At times their time-histories exhibit abnormally large values and even sharp peaks in correspondence of very small slowly-varying mean wind velocity values, sometimes tending to zero. Accordingly, the large I_u and I_v values (greater than 0.2) related to small $\overline{u}$ values (less than 5 m/s) are ignored in the following analyses (Zhang et al., 2019).

Table 5 shows the mean values, $\langle\cdot\rangle$, and the coefficients of variation, cov($\cdot$), of the average longitudinal and lateral slowly-varying turbulence intensities, $\overline{I}_u$ and $\overline{I}_v$, evaluated over the ensemble of the thunderstorm outflow records detected by each anemometer. The mean values of $\overline{I}_u$ and $\overline{I}_v$ decrease on increasing the height whereas their cov values increase on increasing the height. $\langle\overline{I}_u\rangle$ and $\langle\overline{I}_v\rangle$ assume quite similar values because they have been deprived by their low-frequency harmonic content through the mobile mean operator (Zhang et al., 2019). Despite this, $\langle\overline{I}_u\rangle$ is slightly larger than $\langle\overline{I}_v\rangle$.

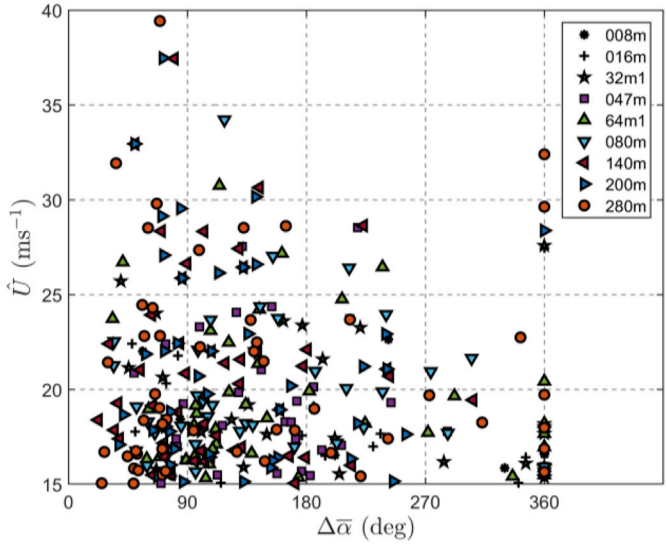

Fig. 13. Peak wind speed $\widehat{U}$ as a function of the direction shift in 30 min.

Table 5
Ensemble mean value and cov of the turbulence intensity.

Anemometer No.	h (m)	$\langle \bar{I}_u \rangle$	cov($\bar{I}_u$)	$\langle \bar{I}_v \rangle$	cov($\bar{I}_v$)
1	8	0.34	0.12	0.30	0.12
2	16	0.27	0.14	0.25	0.17
3	32	0.22	0.22	0.20	0.17
4	47	0.21	0.39	0.19	0.29
5	64	0.20	0.42	0.17	0.24
6	80	0.18	0.34	0.16	0.26
7	140	0.12	0.34	0.10	0.29
8	200	0.10	0.35	0.09	0.33
9	280	0.11	0.88	0.08	0.41

It is relevant to point out that the $\langle \bar{I}_u \rangle$ and $\langle \bar{I}_v \rangle$ values detected by the anemometers 1–4 of the Being Tower, the ones close to the ground, are much larger than those related to the thunderstorm outflows detected at similar heights in the northern Mediterranean. As better discussed below, this may be due to the fact that in the latter case the thunderstorm outflows mainly come from the sea whereas the Beijing tower is embedded in an urban area. In addition, the Mediterranean thunderstorms examined by Zhang et al. (2019) were limited to 10-min rapid events whereas those investigated in this paper include slower 1-h and 10-h events for which more time is available to create a boundary layer flow in equilibrium with the local roughness. Also this topic deserves further investigations.

Fig. 14 **(a)** shows the average values of the turbulence intensity of the thunderstorm outflows as a function of h/z_0 (Xu and Hangan, 2008; Lombardo et al., 2014), where h is the height AGL and z_0 is the roughness length; the latter quantity is estimated referring to neutral synoptic conditions, taking into account the upwind roughness features (GB50009-2012; ESDU, 1993). The difference between the longitudinal and the lateral turbulence intensity is not relevant for most of the records, while the former is definitely larger than the latter for a few isolated thunderstorm outflow records. Similar to the results provided by Zhang et al. (2019), $\bar{I}_u$ and $\bar{I}_v$ decrease on increasing h/z_0; in addition, focusing on turbulence intensities associated with similar values of h/z_0, between 10^1 and 10^2, the agreement with the Mediterranean outcomes is definitely better. Also the decrease of $\bar{I}_u$ and $\bar{I}_v$ on increasing $\bar{u}_{max}$ has strong analogies with the trend provided by Zhang et al. (2019) for the thunderstorms in the northern Mediterranean.

The μ_u and μ_v functions defined by Eq. (3) are also considered. Similar to the results related to the thunderstorm outflows in the northern Mediterranean, both the mean value and the cov of μ_u and μ_v are weakly dependent on time; this means that μ_u and μ_v can be regarded, in simplified terms, as stationary processes. On the other hand, the μ_u and μ_v sample functions are not symmetric with respect to the mean, and their probability density functions (pdf) are detached from the reference Gaussian model, so they constitute a non-Gaussian process. Table 6 illustrates, for all the thunderstorm records considered, the ensemble mean value (Mean) and standard deviation (Std) of the mean value (m), standard deviation (σ), skewness (γ) and kurtosis (κ) of μ_u and μ_v. This strengthens the above remark by pointing out the detachment of the skewness and kurtosis of μ_u and μ_v from 0 to 3, respectively. All these results closely match the ones obtained in the Mediterranean area (see Figs. 18 and 19 and Table 4 of the paper by Zhang et al. (2019)).

6.4. Reduced turbulent fluctuations

The longitudinal and lateral reduced turbulent fluctuations, $\tilde{u}'$ and $\tilde{v}'$, are defined through Eq. (3). Table 7 shows, for all the thunderstorm records considered, the ensemble mean value (Mean) and standard deviation (Std) of the mean value (m), standard deviation (σ), skewness (γ) and kurtosis (κ) of $\tilde{u}'$ and $\tilde{v}'$. Pointing out the reliability of representing these quantities as Gaussian random processes with zero mean and unit standard deviation. Table 8 shows the correlation coefficient of $\tilde{u}'$ and $\tilde{v}'$ for all the thunderstorm records considered. Independently of height, its nearly zero value everywhere confirms that $\tilde{u}'$ and $\tilde{v}'$ are almost fully uncorrelated. All these results are perfectly consistent with the outlines of the analyses carried out in the northern Mediterranean (see Fig. 20 and Tables 5 and 6 of the paper by Zhang et al. (2019)).

6.5. Turbulence integral length scales and power spectral densities

As far as concerns the integral length scale and the power spectral density (PSD) of the longitudinal and lateral reduced turbulent fluctuations, $\tilde{u}'$ and $\tilde{v}'$, a more controlled sub-set of 284 thunderstorm outflow records, including an extremely low number of missing values, has been extracted and investigated; in the very few points in which the time series is interrupted, its continuity has been obtained though linear interpolation.

The longitudinal and lateral integral length scales of the reduced turbulent fluctuations, L_u and L_v, are determined from the autocorrelation function of $\tilde{u}'$ and $\tilde{v}'$ (Zhang et al., 2018a), using the

Table 6
Ensemble Mean value and Std of the mean value (m), standard deviation (σ), skewness (γ) and kurtosis (κ) of μ_u and μ_v.

	Parameter	m	σ	γ	κ
μ_u	Mean	1.000	0.404	0.753	3.399
	Std	0.000	0.132	0.582	1.959
μ_v	Mean	1.000	0.397	0.745	3.366
	Std	0.000	0.128	0.536	1.430

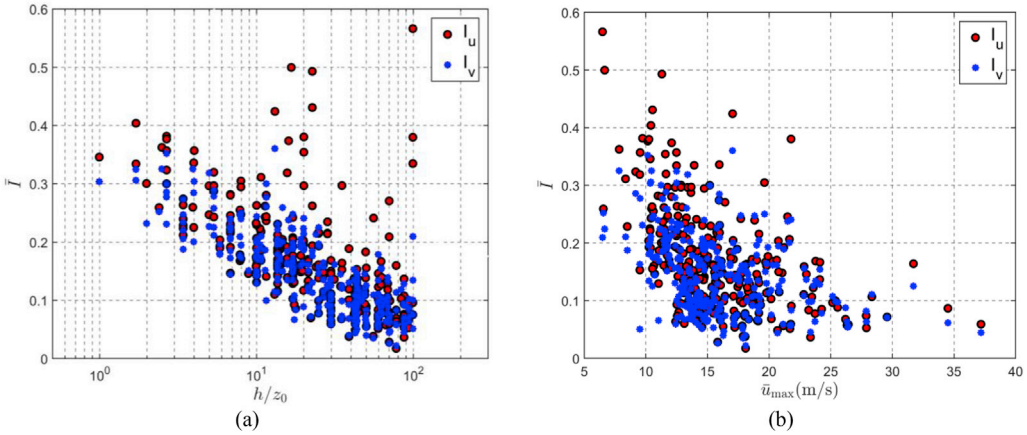

Fig. 14. Average turbulence intensity as a function of h/z_0 (a) and $\bar{u}_{max}$ (b).

Table 7
Ensemble Mean value and Std of the mean value (m), standard deviation (σ), skewness (γ) and kurtosis (κ) of $\tilde{u}'$ and $\tilde{v}'$.

	Parameter	m	σ	γ	κ
$\tilde{u}'$	Mean	0.013	1.005	−0.037	2.895
	Std	0.023	0.012	0.188	0.426
$\tilde{v}'$	Mean	0.000	1.002	0.005	2.909
	Std	0.018	0.010	0.135	0.291

method proposed by Flay and Stevenson (1988). Table 9 shows the mean value and the cov of L_u and L_v as detected by each anemometer. The mean values of both these scales increase on increasing the height AGL whereas their cov exhibit a less regular trend. L_v is slightly lower than L_u. All these estimates are consistent with those obtained in the Mediterranean area (Zhang et al., 2019).

Fig. 15 shows L_u and L_v as a function of h/z_0 **(a)** and $\overline{u}_{max}$ **(b)**. L_u and L_v exhibit a slight increase with h/z_0, which was not pointed out by the analyses carried out in the northern Mediterranean; probably, such trend at the Beijing Tower is made clear by the presence of anemometers up to 280 m height. The Beijing data also show a clear increase of L_u and L_v on increasing $\overline{u}_{max}$; this result matches the classical results for synoptic winds and neutral atmospheric conditions and also the results obtained in the Northern Mediterranean area with regard to thunderstorms (Zhang et al., 2019).

Fig. 16 shows the PSD of $\tilde{u}'$ **(a)** and $\tilde{v}'$ **(b)** as a function of the reduced frequency $f = nL/\overline{u}_{max}$, $\overline{u}_{max}$ being the maximum value of the slowly-varying mean wind velocity, confirming the reliability of the parameterization previously adopted by Zhang et al. (2018b and 2019). In particular, despite the presence of anemometers located in a broad range of different heights, the mean values of the PSD related to each height exhibit one dominant peak whose position is very close to the one determined for the thunderstorm outflows in the northern Mediterranean (see Fig. 23 (b) and (c) of the paper by Zhang et al. (2019)). Fig. 17 compares the PSD of $\tilde{u}'$ and $\tilde{v}'$ as averaged over the ensemble of all the anemometers. It is worth noting that they exhibit an almost perfect superposition, even better than the one obtained with regard to the thunderstorms in the northern Mediterranean (see Fig. 23 (d) of the paper by Zhang et al. (2019)).

6.6. Turbulence intensity modulation

In the light of Eq. (3), though $\tilde{u}'(t)$ and $\tilde{v}'(t)$ are well represented by Gaussian (rapidly-varying) random processes, $\mu_u(t)\tilde{u}'(t)$ and $\mu_v(t)\tilde{v}'(t)$ are non-Gaussian random processes due to the factorization by means of the non-Gaussian (slowly-varying) random processes $\mu_u(t)$ and $\mu_v(t)$. The ensemble mean value and standard deviation of the mean, standard deviation, skewness and kurtosis of $\mu_u(t)\tilde{u}'(t)$ and $\mu_v(t)\tilde{v}'(t)$ are shown in Table 10, which exhibits some differences especially with regard to the higher-order statistical moments. The obtained results also show that the PSD of $\mu_u(t)\tilde{u}'(t)$ exhibits some slight differences from the PSD of $\mu_v(t)\tilde{v}'(t)$, mostly limited to the low-frequency harmonic content; however, the PSDs of $\tilde{u}'(t)$ and $\tilde{v}'(t)$ are very close to the PSDs of their modulations. Also these outcomes perfectly match the results obtained for the thunderstorm outflows in the northern Mediterranean (see Figs. 24 and 25 and Table 8 of the paper by Zhang et al. (2019)).

Table 9
Ensemble Mean value and cov of the integral length scales of the reduced turbulent fluctuation.

Anem. No.	h (m)	$\langle L_u \rangle$ (m)	cov(L_u)	$\langle L_v \rangle$ (m)	cov(L_v)
1	8	16.05	0.24	13.51	0.22
2	16	21.41	0.19	17.19	0.20
3	32	23.68	0.29	19.60	0.27
4	47	23.69	0.29	20.91	0.26
5	64	27.33	0.23	23.75	0.21
6	80	27.70	0.24	23.69	0.22
7	140	30.56	0.31	27.92	0.23
8	200	32.68	0.28	29.65	0.27
9	280	33.49	0.31	32.19	0.31

6.7. Gust factor

The gust factor, G_u, plays a key role in the thunderstorm loading and response of structures (Solari et al., 2015, Solari 2016 and Solari et al., 2017).

Table 11 summarizes the mean value and the cov of G_u. Its mean value exhibits a clear decrease on increasing the height AGL, while there is no apparent correlation between the cov and the height. It is worth noting that the mean values of G_u detected by the anemometers 1–4 of the Being Tower, those close to the ground, are much larger than those related to the thunderstorm outflows detected at similar heights in the northern Mediterranean (Zhang et al., 2019). Similarly to the turbulence intensities, as better explained below, this may be due to the fact that in the latter case the thunderstorms mainly come from the sea whereas the Beijing tower is embedded in an urban area.

Fig. 18 shows the gust factor as a function of h/z_0 **(a)** and $\overline{u}_{max}$ **(b)**, respectively. According to Fig. 18 **(a)**, the gust factor exhibits a slight decrease on increasing h/z_0. Fig. 18 **(b)** shows that the gust factor G_u clearly decreases on increasing $\overline{u}_{max}$. Both these trends match the results of the previous analyses carried out in the northern Mediterranean. In addition, focusing on the gust factors associated with similar values of h/z_0, between 10^1 and 10^2, the agreement with the Mediterranean outcomes is definitely better (see Figures 26 and 27 of the paper by Zhang et al. (2019)).

7. Wind speed time-space structure for a thunderstorm outflow event

Thunderstorm outflows give rise to wind velocity fields that are different from the classical boundary layer wind fields produced by synoptic events. Although many measurements have been carried out of the wind speed in the course of downbursts, most of them are provided by single instruments whereas few simultaneous measurements at the same location are still available to reconstruct the wind field. The ultrasonic anemometers mounted at nine different heights along the meteorological Beijing tower from 8 m to 280 m AGL provide a unique opportunity to inspect the time-space (vertical) structure of the wind fields generated by thunderstorm outflows. In this section, a description of a typical thunderstorm outflow detected on June 10, 2016 is provided. Systematic analyses of the whole dataset are currently in progress and will be illustrated in future papers.

Figs. 19 and 20 show the 1-h time history records registered by the anemometers placed at 64 and 140 m heights. Pictures **(a)**, **(b)** and **(c)** show the time-series of the wind speed, direction and temperature raw

Table 8
Correlation between $\tilde{u}'$ and $\tilde{v}'$ for the thunderstorm records considered.

Anem. No.	1	2	3	4	5	6	7	8	9	All
h (m)	8	16	32	47	64	80	140	200	280	–
Cor($\tilde{u}'\tilde{v}'$)	0.000	−0.032	−0.054	−0.034	0.024	0.049	0.004	0.020	0.048	0.003

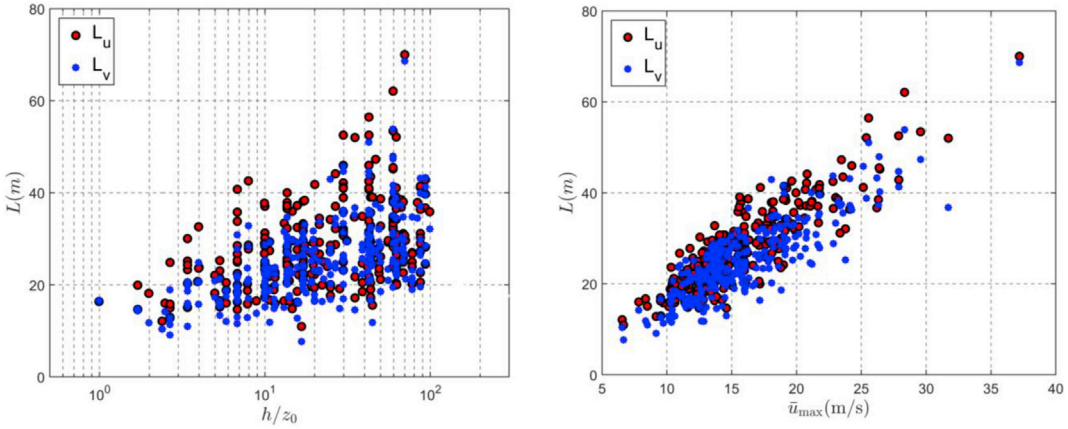

Fig. 15. Integral length scales as a function of h/z_0 (a) and $\bar{u}_{max}$ (b).

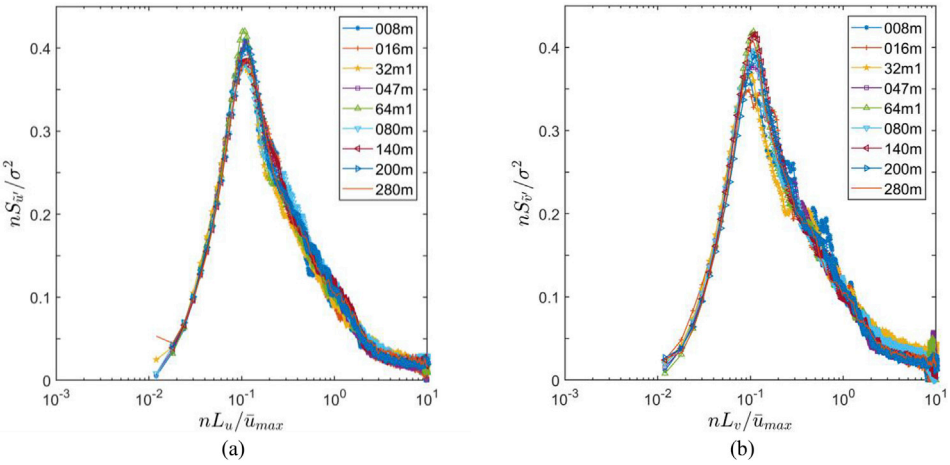

Fig. 16. PSD of $\hat{u}$' (a) and $\hat{v}$' (b) for the mean value of different records for every anemometer as a function of $f = nL/\bar{u}_{max}$.

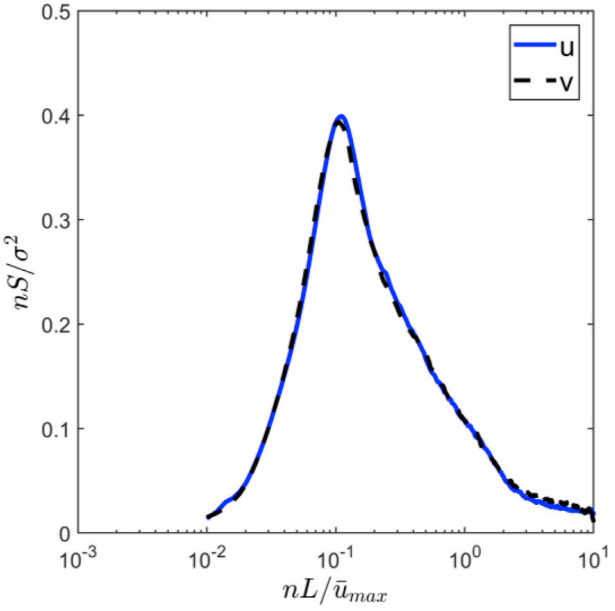

Fig. 17. Mean value of the PSD of $\hat{u}$' and $\hat{v}$' for different records as a function of $f = nL/\bar{u}_{max}$.

data, respectively; they also provide their mean values over 1-h (solid lines), and 10-min (dotted lines) periods. In addition, picture **(a)** shows the 1-s peak wind speed (red circle), the 30 s slowly-varying mean wind velocity (cyan line) and its maximum value (pink square).

The records depicted by Figs. 19 and 20 show a rapid and intense jump of the wind velocity coupled with a direction shift of about 180 deg and a temperature drop of about 5 °C. These typical features of a thunderstorm outflow are strengthened by a careful weather survey that confirmed the simultaneous presence of thunderstorms on the Beijing area.

The following deals with the wind speed profile (section 7.1), the turbulence intensity (section 7.2), and the integral length scale (section 7.3). Spectral analyses are postponed to future papers.

7.1. Wind speed profile

Fig. 21 shows the 30-min time histories of the slowly-varying mean wind speed **(a)** and direction **(b)** at 9 different heights for the thunderstorm outflow examined here. It is worth noting that the sudden and intense jump of the wind speed occurs for all the records, and all of them exhibit evident direction shifts. In particular, a rapid wind rotation clockwise about 200° occurs at around 14:50, when the wind speed begins to increase, followed by a second rapid rotation anti-clockwise about 100° at around 15:09, when the wind speed decreases.

Table 12 shows, for each anemometer, the maximum values of the slowly-varying mean wind speed $\bar{u}_{max}$ and of the peak wind speed $\hat{u}$,

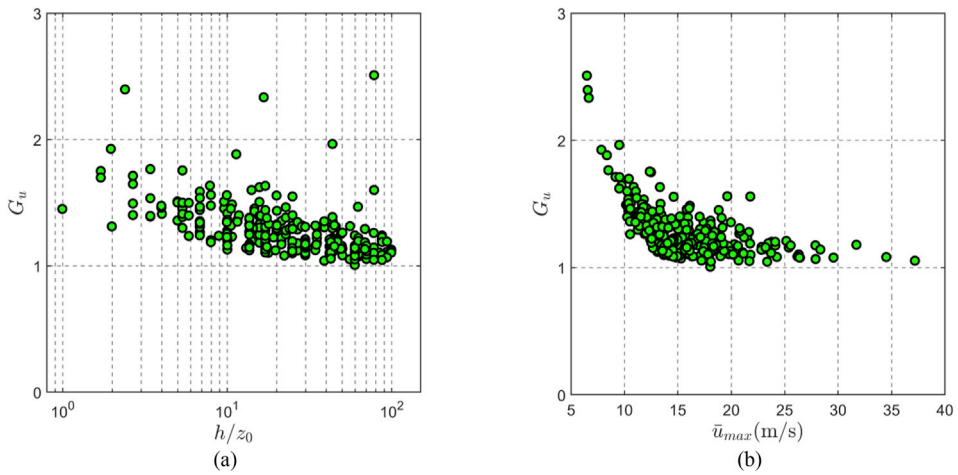

Fig. 18. Gust factor of the thunderstorm outflows as a function of h/z_0 (a) and $\bar{u}_{max}$ (b).

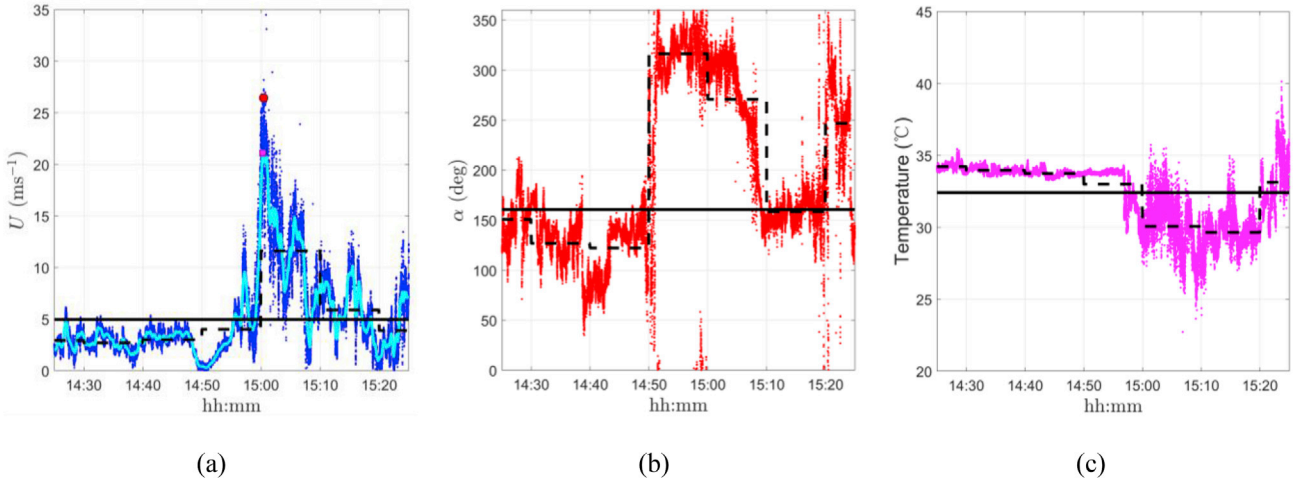

Fig. 19. Thunderstorm outflow recorded on 10 June 2016 by the 64 m anemometer: (a) 1-h wind speed time-series; (b) 1-h wind direction time-series; (c) 1-h temperature time-series.

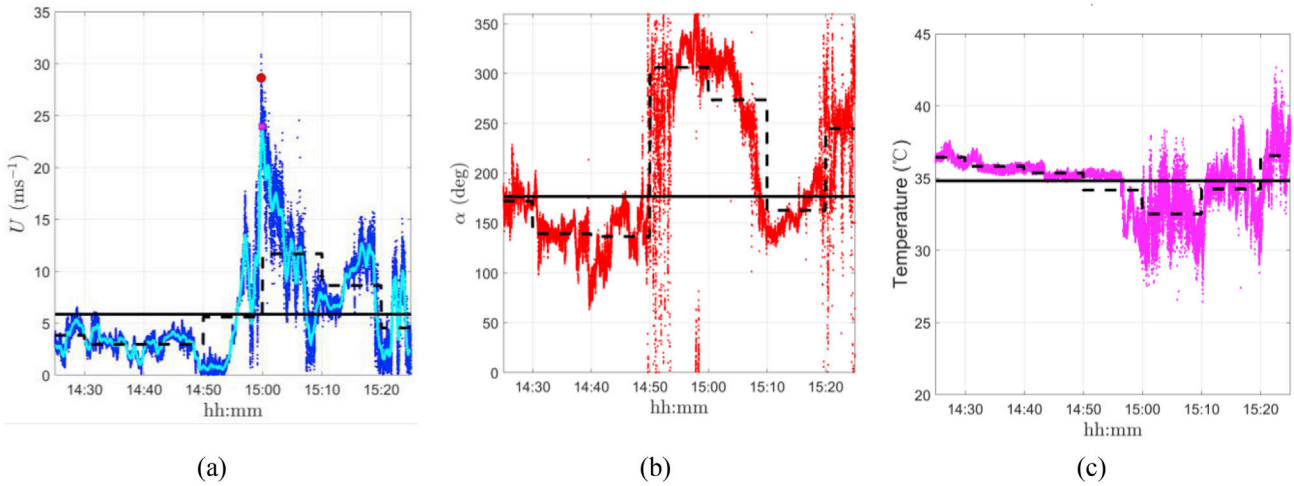

Fig. 20. Thunderstorm outflow recorded on 10 June 2016 by the 140 m anemometer: (a) 1-h wind speed time-series; (b) 1-h wind direction time-series; (c) 1-h temperature time-series.

Table 10
Ensemble Mean and Std values of the mean, standard deviation, skewness and kurtosis (m, σ, γ, κ) of $\mu_u(t)\tilde{u}(t)$ and $\mu_v(t)\tilde{v}(t)$.

	Parameter	m	σ	γ	κ
$\mu_u\tilde{u}$	Mean	0.009	1.106	−0.150	4.874
	Std	0.047	0.064	0.437	2.502
$\mu_v\tilde{v}$	Mean	−0.003	1.098	−0.026	4.694
	Std	0.030	0.059	0.300	1.483

together with their occurrence times, for each anemometer in the 30 min corresponding to Fig. 21. Neither $\overline{u}_{max}$ nor $\widehat{u}$ exhibit a regular trend although $\overline{u}_{max}$ seems to increase with the height more regularly than $\widehat{u}$. The time elapsed between the earliest and latest occurrence of $\overline{u}_{max}$ for the 9 records detected is 64 s (between 200 m and 8 m); similarly, the time elapsed between the earliest and latest occurrence of $\widehat{u}$ is 65 s (between 280 m and 32 m). The time elapsed between $\overline{u}_{max}$ and $\widehat{u}$ for the same record falls in the range between 6 and 14 s for the anemometers up to 140 m height whereas it increases between 41 and 57 s for the two highest anemometers.

Fig. 22 shows the slowly-varying mean wind speed $\overline{u}$ **(a)** and direction $\overline{\alpha}$ **(b)** profiles in the same 30 min depicted in Fig. 21, showing their sudden changes. In particular, at about 15:00, when the spike of the wind speed occurs, Fig. 22 **(a)** points out a rapid colour change that does not correspond to the monotonic increase of the mean wind speed with the height, which is a typical property of a boundary layer wind profile. It is also worth noting, as observed above, that the duration of the spike increases on increasing the height. Fig. 22 **(b)** depicts the two changes of the wind direction that occur at about 14:50 and 15:05; the duration of this directional shift is longer than the corresponding one in terms of wind speed.

Fig. 23 clarifies the evolution of the mean wind speed **(a)** and direction **(b)** profiles, showing them at selected instants. The slowly-varying mean wind speed $\overline{u}$ and direction $\overline{\alpha}$ change slightly with height between 14:45 and 14:49, before the thunderstorm event; in this period, the magnitude of $\overline{u}$ is relatively small and $\overline{\alpha}$ keeps values lower than 180 deg. At the beginning of the ramp-up phase, namely between 14:51 and 14:55, $\overline{u}$ shows a zigzag trend as a function of height, while $\overline{\alpha}$ changes with the time and the height; more precisely, it is larger than 270 deg for the lower heights and smaller than 180 deg for the higher heights. From 14:55 to 14:59, the $\overline{u}$ value related to the higher heights increases quickly while it keeps smaller values for the lower heights; in the meanwhile, $\overline{\alpha}$ assumes values in the range between 270 and 350 deg.

The "nose shape" profile of the slowly-varying mean wind speed (Hjelmfelt, 1988) appears very clearly at 15:00, in proximity of the peak wind speed. At this time, $\overline{u}_{max}$ exhibits its maximum value at 140 m height. Later on the wind speed decreases, the nose shape profile becomes less clear and the height at which $\overline{u}_{max}$ is maximum decreases. After 15:04, the passage of the gust front is mostly concluded. In this period no significant change of direction occurs at different heights. After 15:09, when the mean wind speed becomes very small, the mean wind direction returns to be lower than 180 deg; in particular, it varies a lot with the height near the ground while it keeps almost constant values as the height increases.

The sudden appearance and the rapid dissolution of the nose-shape profile of the slowly-varying mean wind velocity is consistent with the available LiDAR measurements of the thunderstorm outflows detected in the northern Mediterranean (Burlando et al., 2017b).

7.2. Turbulence intensity

Fig. 24 shows the vertical profile of the slowly-varying longitudinal and lateral turbulence intensities, I_u **(a)** and I_v **(b)**, at selected instants densely distributed around the occurrence of the peak wind speed.

Table 11
Ensemble Mean and cov values of the gust factor at different heights.

Anem. No.	1	2	3	4	5	6	7	8	9
h (m)	8	16	32	47	64	80	140	200	280
$\langle G_u \rangle$	1.72	1.47	1.42	1.36	1.30	1.28	1.21	1.15	1.17
Cov(G_u)	0.17	0.09	0.10	0.16	0.09	0.10	0.11	0.07	0.18

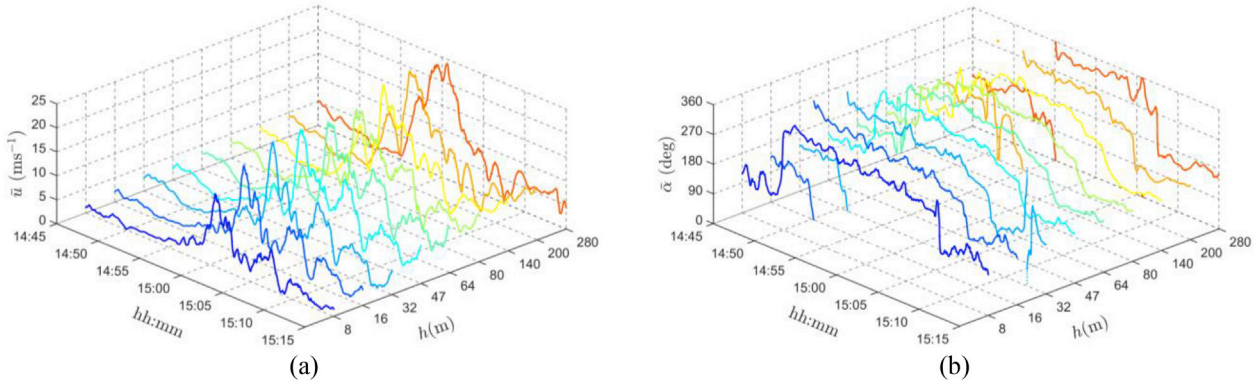

Fig. 21. 30-min slowly-varying wind speed (a) and direction (b) detected by 9 anemometers for a thunderstorm outflow event at June 10, 2016.

Table 12
Maximum values and occurrence time of the moving average wind speed and gust factors for the event.

Anem. No.	1	2	3	4	5	6	7	8	9
h (m)	8	16	32	47	64	80	140	200	280
$\overline{u}_{max}$	15.21	18.82	21.50	21.66	20.81	21.19	23.77	24.12	24.11
$t(\overline{u}_{max})$	15:00:40	15:00:38	15:00:37	15:00:35	15:00:18	15:00:51	14:59:56	14:59:36	15:00:38
$\widehat{u}$	21.29	27.35	27.10	28.25	26.39	26.24	28.60	28.31	28.99
$t(\widehat{u})$	15:00:26	15:00:25	15:00:46	15:00:29	15:00:26	15:00:02	14:59:45	15:00:17	14:59:41

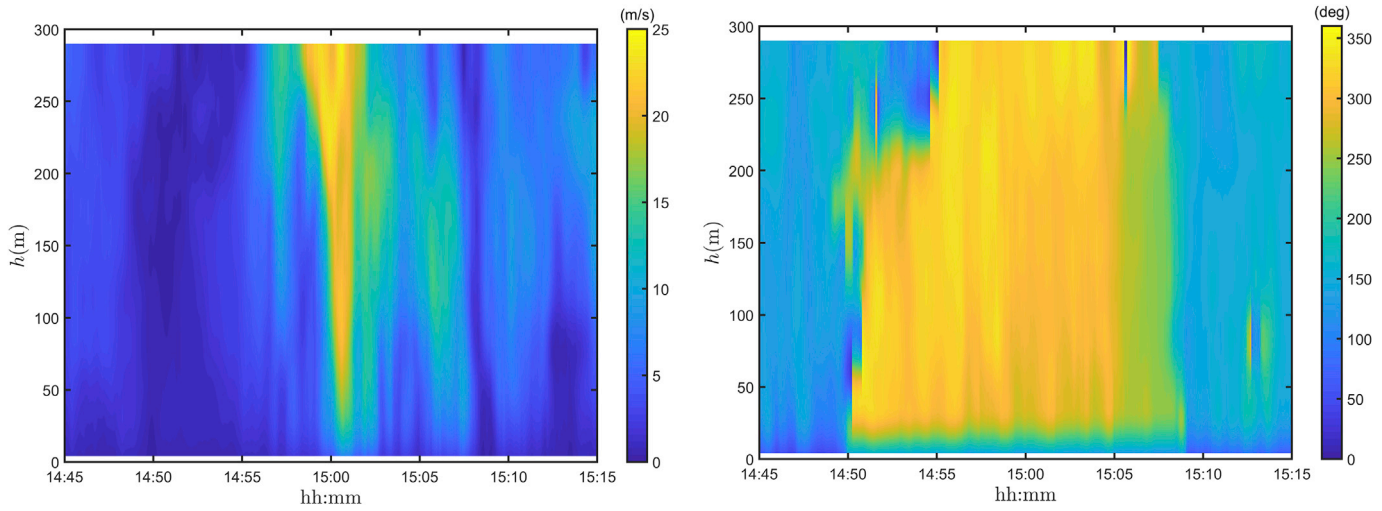

Fig. 22. 30-min time varying wind speed (a) and direction (b) profiles for the thunderstorm outflow event.

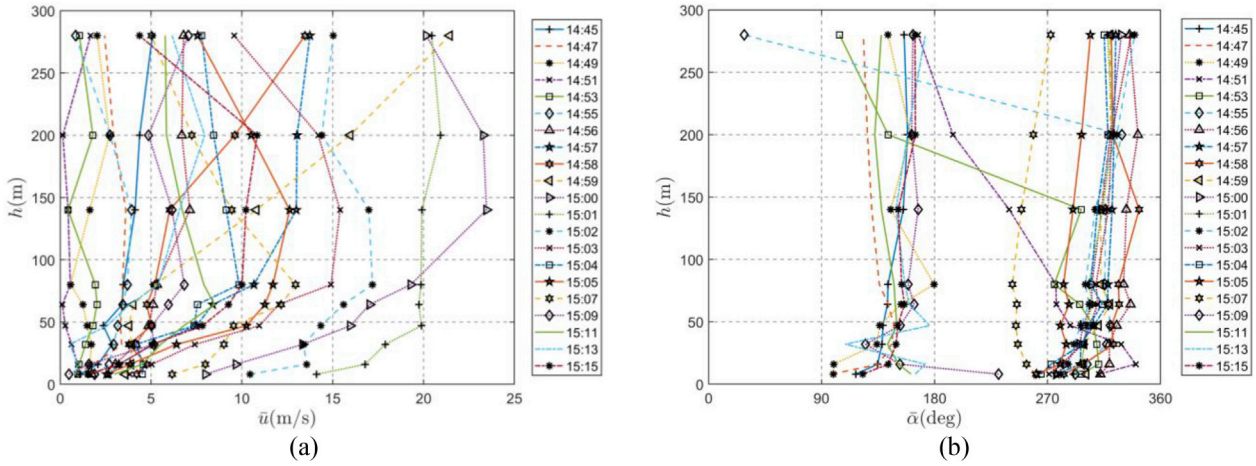

Fig. 23. Mean wind speed (a) and direction (b) profile for the thunderstorm outflow at selected instants.

Fig. 24 shows the vertical profiles of the mean values of I_u **(c)** and I_v **(d)** over the 10-min periods centred on the selected instants. Of course, the latter exhibit a more regular trend and a reduced scatter in values. As described in section 6.3, their abnormal large values and even sharp peaks are disregarded; therefore, in Fig. 24 **(a)** and **(b)**, some values are not present.

In the examined case, I_u **(a)** and I_v **(b)** grow during the passage of the gust front. In this period, they exhibit a zigzag trend with the height, especially close to the ground. As far as concerns $\bar{I}_u$ **(c)** and $\bar{I}_v$ **(d)**, both of them show variable trends close to the ground whereas they decrease on increasing the height. It seems reasonable to assume that the above described behaviour depends on the urban environment and on the average height of the buildings surrounding the Beijing tower.

7.3. Turbulence integral length scale

Fig. 25 shows the vertical profile of the longitudinal and lateral turbulence integral length scales of $\tilde{u}$ and $\tilde{v}$, L_u **(a)** and L_v **(b)**, at the same selected instants used for Fig. 24.

In the examined case, L_u and L_v grow during the passage of the gust front; this behaviour confirms the trend exhibited by Fig. 15 **(b)** according to which L_u and L_v increase on increasing the mean wind speed. In this period zigzag vertical profiles occur along the whole range of the height. On increasing the height, L_v becomes a little bit larger than L_u, while L_u is larger than L_v close to the ground. Probably, this trend depends on the peculiarities of the examined event and by the typical scatter of values exhibited by the integral length scale.

8. Conclusions and perspectives

Currently the engineering-orientated thunderstorm data have been collected from plain, harbour and mountain areas. However, few data have been reported from urban areas. Hence, the thunderstorm data from the Beijing meteorological station provides a good opportunity to fill this gap in the thunderstorm knowledge.

This paper introduces the characteristics of the 325 m high meteorological tower in Beijing and the properties of the anemometers installed over the tower. It describes the Beijing climate and the database generated by nine ultrasonic anemometers placed at different heights from 8 m to 280 m along the tower. It illustrates the procedure used to separate the records associated with different wind phenomena. Thanks to this procedure, 314 records corresponding to 70 events labelled as thunderstorm outflows are selected. They represent a good opportunity to study the properties of the thunderstorm outflows in the Beijing urban area and their main characteristics relevant to wind engineering, with special concern for wind actions on structures. They also provide a unique chance to compare such properties with those of the thunderstorm outflows detected in the northern Mediterranean, and to give a preliminary answer to the crucial question whether thunderstorms have similar properties in different areas, or better what of their properties are

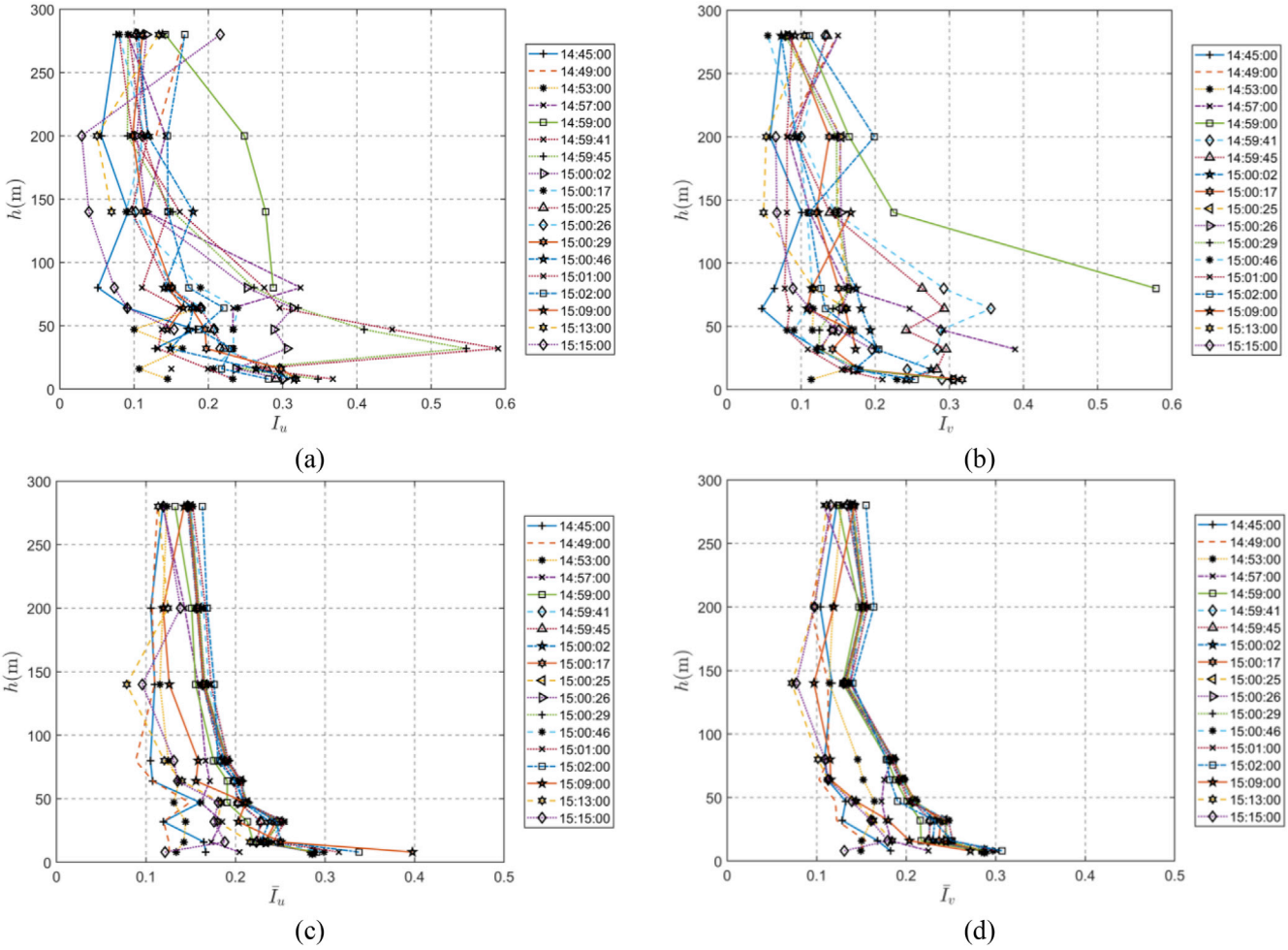

Fig. 24. 30-s slowly-varying turbulence intensity (a) (b) and the 10-min mean turbulence intensity (c) (d) at selected instants for the longitudinal and lateral components.

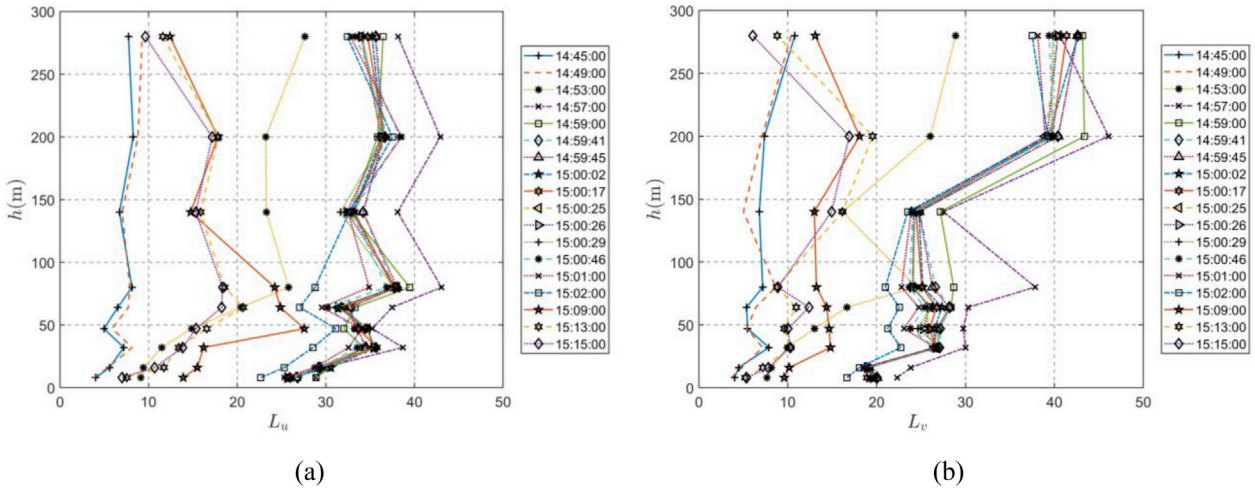

Fig. 25. Longitudinal and lateral integral length scales L_u (a) and L_v (b) as a function of h at selected instants.

similar and what depend on the area itself. Answering to this question is fundamental it order to develop a thunderstorm model possibly shared worldwide. The study is carried out through a new directional signal decomposition strategy, mostly dealing with the records detected by different anemometers as disjoint from each other.

First of all, it is worth noting that the Beijing meteorological tower and the Northern Mediterranean monitoring network have very different properties. They are placed in totally different parts of the planet. The former is embedded in an urban environment and all the instruments are put along a vertical line between 8 and 280 m above the ground level. The latter includes isolated anemometers, mainly placed between 10 and 30 m height, which are distributed along the coast, with the sea on one

side and an urban context on the other, frequently involving complex topographic features. On the other hand, in both the sites the anemometers are ultrasonic sensors with a sampling rate of 10 Hz, a comparable period of measurements, around 5 years, is examined, the gathered records are analysed by means of the same procedure and by the same persons. In their whole, the analyses show some differences, several analogies and many identical trends.

The slowly varying mean wind velocity at the Beijing tower shows the essential features of a ramp-up stage followed by a ramp-down stage corresponding to the passage of a gust front whose duration increases on increasing the height. The analyses show that the overall mean values of the increasing, decreasing and total duration of the most intense part of the thunderstorm are about 143, 190 and 333s, respectively. The minimum values of these three parameters, respectively about 9, 11 and 32s, indicate the possibility that some thunderstorm outflows occur with very rapid variations of the wind velocity.

These results highlight that close to the ground the passage duration of the gust fronts on the Beijing tower is considerable lower than that observed in the Mediterranean at similar heights. The passage duration of the gust front in the Mediterranean (close to the ground) is similar to that observed at the Beijing tower at intermediate heights. This aspect represents one of the main outcomes of this study and deserves further investigations.

The turbulence intensities at the Beijing tower show, close to the ground, much greater values than those observed in the northern Mediterranean; probably, this is due to the fact that in the latter case the thunderstorm outflows mainly come from the sea whereas the Beijing tower is embedded in rougher urban area. Despite this remark, comparing measurements involving similar ratios between the height of the anemometer and the roughness length, the results seem to be much closer between each other. The gust factor exhibit very similar properties. The whole of these results points out an increasing role of the height above the ground level and of the roughness length not fully captured in the Mediterranean area due to the local terrain features and the anemometers siting. This aspect deserves special consideration with reference to the thunderstorm modelling aiming to evaluate the wind loading of structures.

As far as concerns the reduced turbulent fluctuations and their integral length scales and spectral density functions, the similarity between the data detected in the Beijing urban area and in the northern Mediterranean is so strong as to seem almost surprising. In both these cases the reduced longitudinal and lateral turbulent fluctuations are stationary Gaussian and uncorrelated, the integral length scales are weakly influenced by the roughness length but it is sensitive to the wind speed, the parameterization of the power spectral densities as a function of a reduced frequency involving the integral length scale is exceptionally robust. It seems reasonable to assume that these results are favoured and enhanced by the directional decomposition strategy adopted here.

Pending the systematic processing of the entire data base to study the space-time structure of the thunderstorm outflows recorded at the Beijing meteorological tower, some preliminary analyses have been carried out here with respect to a sample thunderstorm event. They show the occurrence of the nose profile of the slowly-varying mean wind velocity for a short time interval in proximity of the peak wind speed. They also show, perhaps for the first time, evolutionary profiles of the turbulence intensities and integral scales that highlight the intensification of these quantities near the peak and confirm the complexity of the phenomenon under examination.

It clearly emerges that the disjoint analysis of single wind speed records provides essential elements for the statistical description of the phenomenon as a function of the height above the ground and of other fundamental parameters such as the intensity of the wind speed and the terrain roughness. On the other hand, this analysis cannot clarify the evolutionary properties of the spatial structure of the thunderstorm outflows, a subject that calls for the simultaneous analysis of the records detected by a densely distributed set of anemometers with high sample frequency, as the instrumentation installed on the Beijing meteorological tower. The perspectives of the present research are just oriented to this study, which represents an essential issue for understanding this physical phenomenon and for evaluating wind actions and effects on structures due to thunderstorm outflows.

National and international co-operation activities are currently in progress to replicate analyses similar to those performed in the Mediterranean area, on the Beijing meteorological tower and in the Chengdu mountainous area in other parts of the world and in terrains with various features, aiming to create a comprehensive architecture of thunderstorms and a better understanding of their characteristics. This is fundamental to carry out in the future better field measurements, including the definition of the tower height and its siting, the allocation of the anemometers and the protocols for the data logging. In parallel, it is highly recommended that these indications may modify the format of the wind acquisitions at official meteorological stations, usually calibrated with regard to synoptic wind and thus ineffective for mesoscale events. All these aspects are strategic to carry out more accurate structural design under thunderstorm outflows, improving the safety and the sustainability of the built environment.

Declaration of Competing Interest

The authors declare that they have no known competing financial interests or personal relationships that could have appeared to influence the work reported in this paper.

Acknowledgement

This work is funded by the National Natural Science Foundation of China (51720105005 and 51778617) and 111 Project of China (B18062, B13002). The third author acknowledges the support of the European Research Council under the European Union's Horizon 2020 research and innovation program (grant agreement No. 741273) for the project THUNDERR – Detection, simulation, modelling and loading of thunderstorm outflows to design wind safer and cost-efficient structures – through an Advanced Grant 2016.

References

Burlando, M., Romanić, D., Solari, G., Hangan, H., Zhang, S., 2017a. Field data analysis and weather scenario of a downburst event in Livorno, Italy, on 1 October 2012. Mon. Weather Rev. 145 (9), 3507–3527.

Burlando, M., De Cio, A., Pizzo, M., Solari, G., 2017b. Analysis of wind vertical profiles of thunderstorm events in the Mediterranean. In: Proceedings of the 9th Asia-Pacific Conference on Wind Engineering Auckland, New Zealand.

Burlando, M., Zhang, S., Solari, G., 2018. Monitoring, cataloguing and weather scenarios of thunderstorm outflows in the Northern Mediterranean. Nat. Hazards Earth Sys 18 (9), 2309–2330.

Chen, L., Letchford, C.W., 2004. A deterministic-stochastic hybrid model of downbursts and its impact on a cantilevered structure. Eng. Struct. 26 (5), 619–629.

Choi, E.C.C., 2000. Wind characteristics of tropical thunderstorms. J. Wind Eng. Ind. Aerodyn. 84, 215–226.

Choi, E.C.C., Hidayat, F.A., 2002a. Dynamic response of structures to thunderstorm winds. Prog. Struct. Eng. Mater. 4, 408–416.

Choi, E.C.C., Hidayat, F.A., 2002b. Gust factors for thunderstorm and non-thunderstorm winds. J. Wind Eng. Ind. Aerodyn. 90, 1683–1696.

Choi, E.C.C., 2004. Field measurement and experimental study of wind speed during thunderstorms. J. Wind Eng. Ind. Aerodyn. 92, 275–290.

Craig Goff, R., 1976. Vertical structure of thunderstorm outflows. Mon. Weather Rev. 104 (11), 1429–1440.

Davenport, A.G., 1961. The application of statistical concepts to the wind loading of structures. In: Proceedings, Institution of Civil Engineers, vol. 19, pp. 449–472.

De Gaetano, P., Repetto, M.P., Repetto, T., Solari, G., 2014. Separation and classification of extreme wind events from anemometric records. J. Wind Eng. Ind. Aerodyn. 126, 132–143.

Duan, Y., Wang, D., Liu, Y., 2017. Radar analysis and numerical simulation of strong convective weather for 'Oriental Star' Depression. J. Appl. Meteorol. Sci. 28 (6), 666–677 (in Chinese).

Durañona, V., Sterling, M., Baker, C.J., 2007. An analysis of extreme non-synoptic winds. J. Wind Eng. Ind. Aerodyn. 95 (9–11), 1007–1027.

Engineering Sciences Data Unit, 1993. Computer Program for Wind Speeds and Turbulence Properties: Flat or Hill Sites in Terrain with Roughness Changes, ESDU Item 92032. London, UK.

Flay, R.G.J., Stevenson, D.C., 1988. Integral length scales in strong winds below 20 m. J. Wind Eng. Ind. Aerodyn. 28, 21–30.
Fu, D.H., Guo, X.L., 2007. Numerical study on a severe downburst-producing thunderstorm on 23 August 2001 in Beijing. Adv. Atmos. Sci. 24 (2), 227–238.
Fujita, T.T., 1985. Andrews AFB Microburst. SMRP Research Paper 205, vol. 38. Universityof Chicago.
Fujita, T.T., 1990. Downbursts: meteorological features and wind field characteristics. J. Wind Eng. Ind. Aerodyn. 36, 75–86.
Geerts, B., 2001. Estimating downburst-related maximum surface wind speeds by means of proximity soundings in New South Wales, Australia. Weather Forecast. 16 (2), 261–269.
Gomes, L., Vickery, B.J., 1977/1978. Extreme wind speeds in mixed climates. J. Ind. Aerodyn. 2, 331–344.
GB50009-2012, 2012. Load Code for the Design of Building Structures. China Architecture & Building Press, Beijing, pp. 31–32.
Gunter, W.S., Schroeder, J.L., 2015. High-resolution full-scale measurements of thunderstorm outflow winds. J. Wind Eng. Ind. Aerodyn. 138, 13–26.
Hjelmfelt, M.R., 1988. Structure and life cycle of microburst outflows observed in Colorado. J. Appl. Meteorol. 27 (8), 900–927.
Holmes, D.J., 2019. Extreme wind prediction – the Australian experience. In: Proceedings of the 15th International Conference of the Italian National Association for Wind Engineering, Naples, Italy (IN-VENTO 2018). Springer, Cham, pp. 365–375.
Holmes, J.D., Oliver, S.E., 2000. An empirical model of a downburst. Eng. Struct. 22 (9), 1167–1172.
Holmes, J.D., Hangan, H.M., Schroeder, J.L., Letchford, C.W., Orwig, K.D., 2008. A forensic study of the Lubbock-Reese downdraft of 2002. Wind Struct. 11, 19–39.
Huang, G.Q., Jiang, Y., Peng, L.L., Solari, G., Liao, H.L., Li, M.S., 2019. Characteristics of intense wind in mountain area based on field measurement. J. Wind Eng. Ind. Aerodyn. 190, 166–182.
Hui, Y., Li, B., Kawai, H., Yang, Q.S., 2017. Non-stationary and non-Gaussian characteristics of wind speeds. Wind Struct. 24 (1), 59–78.
Jarvi, L., Punkka, A.J., Schultz, D.M., Petaja, T., Hohti, H., Rinne, J., Pohja, T., Kulmala, M., Hari, P., Vesala, T., 2007. Micrometeorological observations of a microburst in southern Finland, Bound. La Météorologie 125, 343–359.
Kasperski, M., 2002. A new wind zone map of Germany. J. Wind Eng. Ind. Aerodyn. 90, 1271–1287.
Kwon, D.K., Kareem, A., 2009. Gust-front factor: new framework for wind load effects on structures. J. Struct. Eng. ASCE 135, 717–732.
Letchford, C.W., Mans, C., Chay, M.T., 2002. Thunderstorms – their importance in wind engineering (a case for the next generation wind tunnel). J. Wind Eng. Ind. Aerodyn. 90, 1415–1433.
Li, Q.S., Zhi, L.H., Hu, F., 2009. Field monitoring of boundary layer wind characteristics in urban area. Wind Struct. 12 (6), 553–574.
Liao, X.N., Yu, B., Lu, L.H., 2009. Climatology and nowcasting methods for thunderstorm gale in Beijing. Meteorol. Mon. 35 (9), 18–28.
Liu, H.E., 2001. Characteristics and numerical simulation of microburst. Acta Meteorol. Sin. 259 (2), 183–195.
Lombardo, F.T., Smith, D.A., Schroeder, J.L., Mehta, K.C., 2014. Thunderstorm characteristics of importance to wind engineering. J. Wind Eng. Ind. Aerodyn. 125, 121–132.
Orwig, K.D., Schroeder, J.L., 2007. Near-surface wind characteristics of extreme thunderstorm outflows. J. Wind Eng. Ind. Aerodyn. 95, 565–584.
Qin, L., Li, Y.D., Gao, S.T., 2006. The Synoptic and climatic characteristic studies of thunderstorm winds in Beijing. Climatic Environ. Res. 11 (6), 754–762 (in Chinese).
Riera, J.D., Ponte Jr., J., 2012. Recent Brazilian research on thunderstorm winds and their effects on structural design. Wind Struct. 15 (2), 111–129.
Solari, G., Piccardo, G., 2001. Probabilistic 3-D turbulence modeling for gust buffeting of structures. Probabilistic Eng. Mech. 16, 73–86.
Solari, G., Tubino, F., 2002. A turbulence model based on principal components. Probabilistic Eng. Mech. 17, 327–335.
Solari, G., 2014. Emerging issues and new frameworks for wind loading on structures in mixed climates. Wind Struct. 19, 295–320.
Solari, G., Burlando, M., De Gaetano, P., Repetto, M.P., 2015. Characteristics of thunderstorms relevant to the wind loading of structures. Wind Struct. 20, 763–791.
Solari, G., 2016. Thunderstorm response spectrum technique: theory and applications. Eng. Struct. 108, 28–46.
Solari, G., Rainisio, D., De Gaetano, P., 2017. Hybrid simulation of thunderstorm outflows and wind-excited response of structures. Meccanica 52 (13), 3197–3220.
Solari, G., 2019. Wind Science and Engineering. Springer, Switzerland.
Song, Y.L., Achberger, C., Linderholm, H.W., 2011. Rain-season trends in precipitation and their effect in different climate regions of China during 1961–2008. Environ. Res. Lett. 6 (3), 034025.
Su, Y., Huang, G., Xu, Y., 2015. Derivation of time-varying mean for non-stationary downburst winds. J. Wind Eng. Ind. Aerodyn. 141, 39–48.
Tian, Y., Yang, Q., Yang, N., Li, B., Chen, B., 2011. Statistical spectrum model of wind velocity at Beijing Meteorological Tower. Sci. China Technol. Sci. 54 (11), 2869.
Xu, X.D., Zhang, S., 2019. Property of a typical urban thunderstorm outflow relevant to wind load on structures. IOP Conf. Ser. Earth Environ. Sci. 218 (1), 012086.
Xu, Y.L., Zhan, S., 2001. Field measurements of Di Wang tower during typhoon york. J. Wind Eng. Ind. Aerodyn. 89 (1), 73–93.
Xu, Z., Hangan, H., 2008. Scale, boundary and inlet condition effects on impinging jets. J. Wind Eng. Ind. Aerodyn. 96, 2383–2402.
Yang, N., Bai, F., 2017. Damage analysis and evaluation of light steel structures exposed to wind hazards. Appl. Sci. 7 (3), 239, 2017.
Yang, Q.S., Gao, R., Bai, F., Li, T., Tamura, Y., 2018. Damage to buildings and structures due to recent devastating wind hazards in East Asia. Nat. Hazards 92 (3), 1321–1353.
Zhang, S., Solari, G., De Gaetano, P., Burlando, M., Repetto, M.P., 2018a. A refined analysis of thunderstorm outflow characteristics relevant to the wind loading of structures. Probabilistic Eng. Mech. 54, 9–24.
Zhang, S., Solari, G., Yang, Q.S., Repetto, M.P., 2018b. Extreme wind speed distribution in a mixed wind climate. J. Wind Eng. Ind. Aerodyn. 176, 239–253.
Zhang, S., Solari, G., Burlando, M., Yang, Q.S., 2019. Directional decomposition and properties of thunderstorm outflows. J. Wind Eng. Ind. Aerodyn. 189, 71–90.